



HAL
open science

Experimental study of the influence of hydrogen as a fuel additive on the formation of soot precursors and particles in atmospheric laminar premixed flames of methane

Hong-Quan Do, Luc-Sy Tran, Laurent Gasnot, Xavier Mercier, Abderrahman El Bakali

► To cite this version:

Hong-Quan Do, Luc-Sy Tran, Laurent Gasnot, Xavier Mercier, Abderrahman El Bakali. Experimental study of the influence of hydrogen as a fuel additive on the formation of soot precursors and particles in atmospheric laminar premixed flames of methane. *Fuel*, 2020, pp.119517. 10.1016/j.fuel.2020.119517 . hal-03008298

HAL Id: hal-03008298

<https://hal.science/hal-03008298>

Submitted on 16 Nov 2020

HAL is a multi-disciplinary open access archive for the deposit and dissemination of scientific research documents, whether they are published or not. The documents may come from teaching and research institutions in France or abroad, or from public or private research centers.

L'archive ouverte pluridisciplinaire **HAL**, est destinée au dépôt et à la diffusion de documents scientifiques de niveau recherche, publiés ou non, émanant des établissements d'enseignement et de recherche français ou étrangers, des laboratoires publics ou privés.

1 **Experimental study of the influence of hydrogen as a fuel**
2 **additive on the formation of soot precursors and particles**
3 **in atmospheric laminar premixed flames of methane**

4
5 Hong Quan Do, Luc-Sy Tran, Laurent Gasnot, Xavier Mercier*, Abderrahman El Bakali*

6
7
8 *Physicochimie des Processus de Combustion et de l'Atmosphère (PC2A), CNRS UMR 8522,*
9 *Université de Lille, F-59000 Lille, France*

10
11
12 **Full-Length Article**

13
14
15 **Supplemental Material (SM) is available:**

16 SM1: Additional information (PDF file)

17 SM2: Experimental data (Excel file)

18
19 * Corresponding authors:

20 Prof. Dr. Abderrahman El Bakali

21 Email: abderrahman.el-bakali@univ-lille.fr

22 Dr. Xavier Mercier

23 Email: xavier.mercier@univ-lille.fr

29 **Abstract**

30 We report here the experimental investigation of lightly sooting methane premixed flames
31 with and without hydrogen. Two different approaches were considered to introduce hydrogen
32 in the methane flame, either by keeping the total gas flow rate constant or not. Speciation data
33 were obtained using a set of analytical tools including Gas Chromatography, Fourier-
34 Transform Infrared Spectroscopy, Jet-Cooled Laser-Induced Fluorescence, Laser-induced
35 Incandescence coupled with Cavity Ring-Down Spectroscopy.

36 The results include mole fraction profiles of gaseous species (C_0 - C_{16}) and soot volume
37 fraction (f_v) measured in all studied flames. These results demonstrate that the introduction of
38 hydrogen to the flame insignificantly impacts the maximum mole fractions of small species
39 ($<C_6$) while it strongly influences the concentration of aromatics and f_v . Interestingly, this
40 influence is different, depending on how hydrogen was added to the reference methane flame.
41 An excellent linear relationship between pyrene squared concentrations $[C_{16}H_{10}]^2$ and f_v is
42 demonstrated in all investigated flames. Moreover, hydrogen addition changes the slope of
43 these data indicating a non-negligible impact of hydrogen on the rate of the soot nucleation
44 process. These data and the observed linearity between f_v and $[C_{16}H_{10}]^2$ supports therefore the
45 idea of a soot nucleation step **initiated** by a dimerization process implicating moderate-size
46 **polyaromatic hydrocarbons** (PAHs) as pyrene. Finally, we note that PAH mole fractions at the
47 beginning of soot formation highlight similar values regardless the flame conditions, which
48 suggests that the inception of the soot formation might be dependent of a minimum
49 concentration threshold of aromatic precursors required to initiate the soot nucleation process.

50

51 **Keywords:** Hydrogen; Methane; Premixed flame; PAHs; Soot nucleation; Soot

52

53 **1. Introduction**

54 Energy is **necessary for** almost all industrial **and** domestic activities and around 80% of the
55 primary energy **currently** used in the world comes from fossil fuels [1,2]. The world energy
56 demand is growing around 2.3% per year. This increasing energy consumption **not only**
57 contributes to pollution and environmental deterioration **but also to the** global warming and
58 climate change **mostly due to** CO₂ emissions [3,4]. Furthermore, **concomitant formation of**
59 **carbon monoxide (CO), polycyclic aromatic hydrocarbons (PAHs) and soot particles** in real
60 combustion processes (especially those **involving** fuel-rich mixtures), severely affect **the**
61 human health by damaging the cardiovascular system, weakening the immune system and
62 impairing the lung functions [5,6].

63 These challenges have motivated researchers to investigate environmentally friendly
64 alternative fuels. In that context, hydrogen (H₂) is emerging as a zero-carbon energy source
65 with low ignition energy, large flammable range and high burning velocity [7–9]. Mixtures of
66 H₂ with natural gas, primarily **consisted** of methane (CH₄), usually called “hydrogen-enriched
67 natural gas” (HENG), are low-carbon fuel mixtures and being proposed as promising
68 alternative fuels in automotive engines, gas turbines **as well as industrial and** domestic flame
69 burners [10–15]. To support the development of clean and efficient HENG energy systems,
70 fundamental studies are particularly important, notably to improve our knowledge regarding
71 the co-combustion properties of H₂ and CH₄. Hence, some studies were previously **carried out**
72 regarding the influence of H₂ as a fuel additive on the global combustion properties of CH₄.
73 For example, the local flame extinction, combustion stability and power output of CH₄
74 combustion were found to be improved with H₂ enrichment [16,17]. Moreover, it has been
75 demonstrated that the thermal and chemical effects of H₂ addition increased significantly the
76 flame dynamics and combustion efficiency of premixed CH₄ flames [18,19]. **Furthermore, the**

77 adding of high fraction of H₂ to a CH₄ flame has been shown to exponentially increase the
78 laminar burning velocity [20].

79 The impact of H₂ on the formation of soot precursors and soot particles have also been the
80 subject of numerous fundamental studies but mostly for mixtures of H₂ with fuels other than
81 CH₄ [21–37]. By contrast, only a few similar studies, to the best of our knowledge, were
82 addressed to characterize the impact of H₂ on the combustion of CH₄ flames [38–41]. Liu *et*
83 *al.* [38] and Xu *et al.* [39] studied the effects of H₂ as a fuel additive (up to 40% comparing to
84 the base fuel) on soot formation in diffusion CH₄ flames and showed that the addition of H₂
85 strongly decreases the formation of soot. Ezenwajiaku *et al.* [41] also investigated the impact
86 of H₂ (added up to 20% in CH₄) on the formation of PAHs also in a diffusion flame. The
87 authors studied the formation of PAHs by recording their Laser Induced Fluorescence (LIF)
88 signals collected in the wavelength range 420-480 nm after 283 nm excitation. The measured
89 LIF signal was attributed in this work to the global contribution of PAHs constituted of 3-5
90 aromatic rings. The authors found this way that the use of H₂ as a fuel additive decreased the
91 amounts of such classes of PAHs. However, those experiments did not enable the selective
92 identification of these PAHs. Mze Ahmed *et al.* [40] experimentally and numerically studied
93 the impact of added H₂ (40% in CH₄) in a premixed laminar sooting flame of methane
94 (equivalence ratio relative to CH₄ $\Phi_C=2.2$) and found that the presence of H₂ in the mixtures
95 promoted the formation of aliphatic C₁-C₄ species as well as benzene and toluene.

96 However, besides these few reported works, we note that significant specific experimental
97 data listed below are missing in the literature regarding the formation of PAHs and soot in
98 H₂/CH₄ mixture flames. First, no study has ever been published reporting experimental
99 quantification of *individual PAHs* such as naphthalene and pyrene in H₂/CH₄ mixture flames,
100 while these compounds are expected to be key species in the soot formation process. Second,
101 species profiles determined at soot nucleation conditions in H₂/CH₄ mixture flames have

102 never been reported either, while such data are crucial for validating kinetic models and
103 investigating the influence of H₂ in the soot nucleation process. Finally, systematic studies
104 reporting experimental concentration profiles of both gaseous species and solid particles in
105 flames of H₂/CH₄ mixtures remain very scarce while they are of high value to improve our
106 understanding of the co-combustion process of these two fuels and related emissions of PAH
107 and soot.

108 Hence, the main objective of this reported work is to fill in this gap and shed new light on
109 the role of H₂ in the soot formation, with a specific focus on the soot nucleation process. To
110 this aim, a specific advantage has been taken from the choice of the studied flames, defined as
111 nucleation flames, *i.e.* flames in which soot only undergoes very slight or even no growth
112 process along the flame height. This property, which can be reached by finely adjusting the
113 equivalent ratio of the flame as explained below, allows the specific study of the nucleation
114 process without being blurred by the growing processes of soot particles that usually take
115 place in standard sooting flames. Two different approaches were employed to introduce H₂ to
116 the reference flame, consisting either in keeping constant or slightly increasing the total flow
117 rate of the gases. Measurements of both gaseous and solid phase species are reported in this
118 work. Hence, profiles of mole fraction species including selected aliphatic and aromatic
119 compounds (C₀-C₁₆) as well as soot volume fractions were obtained using a combination of
120 complementary highly sensitive optical techniques and analytical tools. A discussion is finally
121 proposed regarding the crucial role of H₂ in the nucleation step of the soot formation and
122 hypothetical associated mechanisms implicated in this process.

123 2. Experimental methods

124 A laminar premixed flame burner and different experimental techniques were used to carry
125 out this work. These techniques include (i) Gas Chromatography (GC) for the detection of
126 fuel and C₁-C₆ species, (ii) Fourier-Transform Infrared Spectroscopy (FTIR) for CO₂ and H₂O

127 profiles, (iii) Jet Cooled Laser Induced Fluorescence (JCLIF) for the quantification of PAHs
 128 and (iv) Laser Induced Incandescence (LII) coupled with Cavity Ring-Down Spectroscopy
 129 (CRDS) for the measurement of soot volume fraction profiles. These techniques are described
 130 in the next sections.

131

132 2.1. Burner and flame conditions

133 Three atmospheric pressure premixed flames were stabilized on a water-cooled McKenna
 134 burner with a bronze porous disk (6 cm diameter). The system was already described
 135 previously [40]. In the present study, the water-cooling circuit was kept at 296 K and a
 136 nitrogen flow, introduced in the co-annular porous of the burner, was set at 1440 NLPH
 137 (normal liter per hour) to protect the flame from the perturbation of the surrounding air. The
 138 conditions of the studied flames are summarized in Table 1.

139

140

141

142 **Table 1.** Experimental conditions. Flame name: Φ -1.82: CH_4 flame; Φ -1.82_H₂-S: CH_4 substituted-H₂
 143 flame; Φ -1.82_H₂-A: CH_4 added-H₂ flame. T_{adia} : adiabatic temperature calculated using GASEQ
 144 program [42]. $T_{uncorrected}$: measured temperature by using a type B thermocouple without correction of
 145 radiative heat loss. NLPH: normal liter per hour.

	Flame		
	Φ -1.82	Φ -1.82_H ₂ -S	Φ -1.82_H ₂ -A
Φ_C	1.82	1.82	1.82
Φ_{C+H}	1.82	1.86	1.86
C/O	0.455	0.455	0.455
Total flow rate (NLPH)	721.4	721.4	734.6
X_{CH_4}	0.184	0.184	0.181
X_{O_2}	0.202	0.202	0.199
X_{N_2}	0.614	0.595	0.602
X_{H_2}	0	0.018	0.018
T_{adia} (K)	1820	1821	1805
$T_{uncorrected}$ (K)	1532	1556	1512
Flame speed at 298 K and 1 atm (cm/s)	8.79	9.50	8.82

146

147 The premixed CH₄ flame (Φ -1.82) was chosen as the reference flame. This particular
148 flame was defined as a “nucleation” flame, *i.e.* a flame producing very small amounts of soot
149 particles that do not undergo or **very limited surface growth** along the height above the burner
150 [43–46]. As previously demonstrated [43,47], soot formation in this kind of flame is
151 dominated by the soot nucleation process while soot growth processes are very limited or
152 efficiently counterbalanced by oxidation or reversible nucleation **processes**. Therefore,
153 introducing H₂ into **such a** nucleation flame provides an excellent opportunity to specifically
154 investigate the soot nucleation process **involved in the** combustion of H₂/CH₄ mixtures **and to**
155 **highlight the influence** of H₂ **with** key species implicated in this process. It is to be noted that
156 the experimental conditions allowing the stabilization of the Φ -1.82 nucleation flame have
157 been determined using the LII technique as described latter in the paper according to a similar
158 protocol used in different recent studies [44–46].

159 There are currently several approaches to investigate the impact of H₂ in flames. In this
160 work, we defined two different ways of introducing H₂ without significantly affecting the
161 flame burned-gas temperature. The first approach is characterized by a “**H₂ substitution**” and
162 corresponds to the flame Φ -1.82_H₂-S. In this case, a small amount of the nitrogen dilution,
163 equal to 10% of the CH₄ flow rate, is subtracted from the reference flame, and a
164 corresponding amount of H₂ is added to the initial gas flow preserving a constant total flow
165 rate. The second approach corresponds to a “**H₂ addition**” and is denoted as flame
166 Φ -1.82_H₂-A. In this case, a small amount of hydrogen, still equal to 10% of the CH₄ flow
167 rate, is directly added to the initial gas flow, therefore slightly increasing the total flow rate
168 (less than 2%) of the flame compared to that of the reference flame. We admit that these latter
169 conditions are not ideal for identifying a H₂ kinetic effect because the total flow is necessarily
170 modified. **However**, the main objective of these latter conditions was to generate a different

171 perturbation on the **gaseous precursors** and **soot particles**, more specifically at the very
172 beginning of the zone of the soot formation.

173 Note that these two approaches do not change the initial carbon and oxygen content. The
174 choice of introducing a small amount of H₂ to the reference flame **has been made** to avoid a
175 significant change of the temperature profiles in the soot formation zone of the different
176 flames. The gas flow rates were measured by using regulated mass flow controllers
177 (Bronkhorst) with a mass flow accuracy of $\pm 0.5\%$. The C, O and H balances were checked to
178 be close to 100% as detailed in Table S1 of the Supplemental Material 1 (SM1).

179

180 **2.2. Analytical techniques**

181 **2.2.1. Flame temperature measurements**

182 Flame temperature profiles were measured with a Pt/Rh(6%)-Pt/Rh(30%) type B
183 thermocouple (diameter 100 μm). The thermocouple was coated with a ceramic layer of
184 BeO–Y₂O₃ to reduce catalytic effects [48]. Errors in the peak temperatures were estimated to
185 be ± 100 K.

186

187 **2.2.2. Measurements of gaseous species**

188 **2.2.2.1 Gas chromatography (GC):**

189 GC was used to identify and quantify aliphatic species and benzene. The GC and sampling
190 system was previously detailed in [49]. A schematic diagram of the used GC setup is
191 available in SM1 (Fig. S1). Briefly, gas samples were extracted from the flames by a quartz
192 sampling microprobe and then directly sent into a low-pressure injection system **connected to**
193 **the** GC CP–3800 Varian. In this experiment, the microprobe (350 μm orifice) was fixed and
194 the burner height was adjustable along the vertical axis, allowing the sampling of species from
195 different heights above the burner. **We chose to use this microprobe with a relatively large**

196 orifice (350 μm) comparing to usual microprobes generally used for non-sooting flame
197 studies (150 μm) in order to limit the soot clogging issues during the sampling of the species.
198 Moreover, as discussed later, the flames studied in this work generated only small soot
199 particles characterized by small volume fractions ($f_v < 1 \times 10^{-10}$). Hence, our sampling
200 experiments were not affected by clogging problems.

201 Two columns (a HP-Plot Al_2O_3 Capillary and a Molecular Sieve 5A) and two detectors (a
202 Flame Ionization Detector (FID) and a Thermal Conductivity Detector (TCD)) were used to
203 analyze chemical species sampled from the flames. Gaseous commercial cylinder calibration
204 mixtures (Air Product) with a mole fraction uncertainty of $\pm 0.5\text{--}2\%$ have been used to
205 calibrate the GC gaseous species analyzed in the present work. The FID and TCD detection
206 limits were respectively about 0.1 ppm and 10 ppm. The mole fraction uncertainty of gaseous
207 species measured by GC in this study is estimated to be less than $\pm 5\%$ for the major species
208 and $\pm 10\%$ for the minor ones.

209

210 **2.2.2.2 Fourier-transform infrared spectroscopy (FTIR):**

211 Fourier-transform infrared spectroscopy (FTIR) with a spectrometer NEXUS THERMO-
212 OPTEK was used to measure CO_2 and H_2O mole fractions profiles. The FTIR system was
213 detailed previously in [11,50] and a schematic diagram of this system is available in SM1
214 (Fig. S2). Gas sample were extracted from the flames using the same microprobe as for GC
215 analyses. The sampling line was heated at 100 $^\circ\text{C}$ to avoid water condensation. A rotary valve
216 pump (flow $2.5 \text{ m}^3\text{h}^{-1}$) allowed the sampling (40 Torr) and conveyed it to a 2-liter heated gas
217 FTIR cell (100 $^\circ\text{C}$) combined with the FTIR apparatus. To avoid the soot deposition on the
218 optical system inside the IRTF gas cell, two filters (QFF, Pall Tissuquartz QAT-UP 2500)
219 were placed before the inlet of the FTIR cell to separate the soot particles from gas sample.
220 The effect of the filters on water condensation was checked. We did not observe any water

221 condensation caused by the use of these filters. The chemical species in the gas sample were
222 analyzed at the time of their passage in the FTIR cell according to an optical path of 10 m.
223 Fifteen scans were realized with a spectral resolution of 1 cm^{-1} . The FTIR spectra was
224 recorded by OMNIC/QUANTPAD software. The selected spectral zone was chosen at 2394-
225 2276 cm^{-1} for CO_2 measurement and $1719\text{-}1698\text{ cm}^{-1}$ for H_2O measurement. The calibration
226 was performed using homemade mixtures of different known compositions of H_2O and CO_2 .
227 The uncertainties on CO_2 and H_2O mole fraction were estimated about $\pm 12\%$ and $\pm 11\%$
228 respectively.

229

230

231 **2.2.2.3 Jet Cooled Laser Induced Fluorescence (JC-LIF):**

232 The determination of the mole fraction profiles of two important PAHs (naphthalene and
233 pyrene) has been carried out by Jet Cooled Laser Induced Fluorescence (JCLIF). A schematic
234 diagram of the corresponding experimental setup is shown in SM1 (Figs. S3, S4). The system
235 was previously detailed in [51–53]. Briefly, JCLIF measurements were carried out after the
236 sampling of the species from the flame thanks to the same microprobe as used for the GC
237 experiments. The whole transfer line from the microprobe down to the analysis chamber was
238 kept at quite low pressure (15 Torr) and heated up to $100\text{ }^\circ\text{C}$ to limit the condensation of the
239 PAHs [54]. Sampled species from the flame were then directly cooled-down (to around 100
240 K) inside an expanded free jet generated in a low-pressure analysis chamber. JCLIF
241 measurements were done directly inside the free jet in this chamber. At such low temperature,
242 the spectra of the sampling PAHs simplify and highlight specific spectral structures enabling
243 their selective detection by LIF. In the absence of collisions inside the free jet, LIF signals can
244 then be calibrated by introducing pure PAHs with known concentrations inside the free jet
245 [52,53].

246 The laser system we used consisted of a Quantel Nd: YAG laser, pumping a dye laser
247 (TDL70 Quantel) with the 2nd harmonic at 532 nm. Two different mixtures of Rhodamine
248 640 and DCM solved in ethanol were used for the oscillator and amplifier of the dye laser to
249 generate by frequency doubling, a laser pulse tunable either in the wavelength range 300-315
250 nm or 315-340 nm. The first dye mixture was used to selectively excite the naphthalene
251 species around 308.2 nm [54] while the second dye mixture was used to excite the pyrene
252 molecules around 321 nm [52]. The laser beam was spatially reduced to a diameter of
253 approximately 1 mm with a system of two pinholes and slightly focus into the center of the
254 analysis chamber with a converging lens ($f=50\text{cm}$). The energy was adjusted around 0.048 J
255 cm^{-2} to be in the linear regime of fluorescence. Fluorescence emission spectra were recorded
256 via an imaging spectrometer (Horiba iHR320 - 300 mm focal length - gratings with 300 gr
257 mm^{-1}) which can be coupled either to a 16-bit intensified charge coupled device camera
258 (Roper Pimax II) or a photomultiplier (Photonis XP2020Q). The conditions of excitation and
259 collection wavelengths for the present measurement of naphthalene and pyrene are
260 summarized in Table S2 (SM1). The uncertainty in naphthalene and pyrene mole fraction was
261 estimated around $\pm 13\%$.

262

263 **2.2.3. Soot species measurements:**

264 **2.2.3.1 Laser Induced Incandescence (LII):**

265 Laser Induced Incandescence (LII) was used in this work for two different purposes, which
266 was (i) the identification of the “nucleation flame” conditions and (ii) the determination of the
267 soot volume fraction profiles in the different flames. A schematic of the LII setup we used for
268 this study is reported in SM1 (Fig. S5). The system was previously detailed in [44,45] and
269 will be only briefly described here. LII experiments have been carried out by using 1064 nm
270 laser excitation wavelength generated by a Nd: YAG (Quantel) at 10 Hz to heat the soot

271 particles. 1064 nm laser excitation wavelength was used to avoid the excitation of PAHs also
272 formed in the flames [55]. The laser beam was expanded into a collimated horizontal plane
273 using two cylindrical lenses ($f_1 = -50$ mm, $f_2 = 200$ mm) and then passed through a
274 rectangular slit (5.96 mm (vertical) \times 0.61 mm (horizontal)) and a converging lens ($f_3 = 200$
275 mm) in order to provide a top-hat irradiance profile at the position of the LII collection
276 volume. During these experiments, the laser energy was continuously monitored with a
277 powermeter located after the burner. The LII signal was collected at right angle of the laser
278 axis with two converging lenses ($f_4 = 25$ cm and $f_5 = 20$ cm) and focused on the collection slit
279 (0.6 mm (vertical) \times 6 mm (horizontal)). LII signals were measured after the collection slit by
280 a photomultiplier Hamamatsu R2257 (PMT). An interference filter centered at 532 ± 9.8 nm
281 was positioned in front of the PMT in order to limit parasite emission and scattering light
282 from the flame. The LII signals recorded by the PMT were acquired and digitized by an
283 oscilloscope Lecroy HDO - 4104A. Before the determination of the LII profiles, fluence
284 curves were determined for different heights above the burner by recording the evolution of
285 the collected LII signal vs laser energy. From these data, a laser fluence of 0.415 J cm^{-2} , *i.e.*
286 under the soot sublimation threshold, was chosen for the measurement of the LII profiles.

287

288 **2.2.3.2 Cavity Ring-Down Spectroscopy (CRDS):**

289 The LII profiles were then calibrated into soot volume fraction profiles by an extinction
290 measurement carried out by CRDS. To this aim, the soot absorption function $E(m)$ was
291 chosen equal to a constant value of 0.25 as previously determined for nascent soot particles
292 studied in comparable nucleation flames [56]. A schematic diagram of this system is available
293 in SM1 (Fig.S6). The flame was positioned at the center of cavity. The CRDS experiments
294 have been carried out by using a 1064 nm laser excitation wavelength generated by a Nd:
295 YAG (Quantel) at 10 Hz to avoid absorption from gaseous PAHs formed in **the flames**. The

296 laser beam was shaped to match the TEM₀₀ traverse electromagnetic mode of the cavity
297 thanks to two converging lenses with similar focal length ($f=10$ cm) and a set of two pinholes.
298 The CRDS cavity consisted of two identical 25-mm-diameter plano-concave mirrors (radius
299 of curvature: 25 cm, separated by distance of 40cm, coated to achieve a high reflectivity of R
300 = 99.96% at 1064nm). The laser beam diameter was estimated to be around 300 μ m and nearly
301 constant along the flame diameter. The light transmitted by the second mirror was collected
302 by a photomultiplier Hamamatsu R2257. A filter RG 780 was placed in front of the PMT to
303 limit the background emission from the flame. The signals were acquired and digitized by an
304 oscilloscope Lecroy HDO - 4104A. The experimental signal was exponentially fitted by a
305 homemade Labview routine to determine the lifetime of the pulse inside the cavity. The
306 uncertainty regarding the soot volume fraction was estimated to be about $\pm 21\%$ in the soot
307 starting zone and $\pm 8\%$ in the post flame region.

308 **3. Results and discussion**

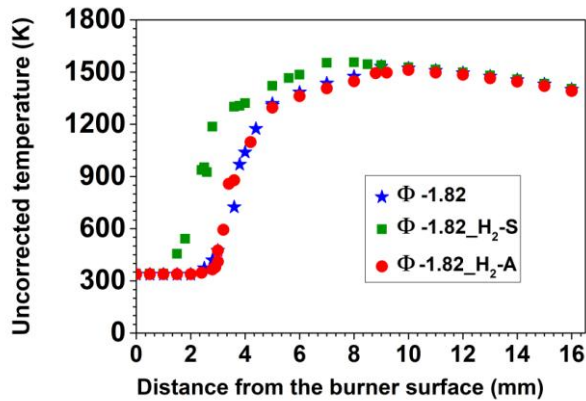
309 The impact of H₂ on temperature and major species (*i.e.* fuel, O₂, CO, CO₂, H₂, H₂O) are
310 addressed in Sections 3.1 and 3.2, respectively. This impact on soot precursors (C₂-C₁₆
311 species) and soot particles (LII decay time, first appearance of the nascent soot particle,
312 relationship between PAHs and nascent soot particles) is discussed in Sections 3.3 and 3.4,
313 respectively.

314

315 **3.1. Impact of hydrogen on flame temperature**

316 Figure 1 shows the experimental uncorrected temperature profiles of the three studied flames
317 (Φ -1.82, Φ -1.82_H₂-S, and Φ -1.82_H₂-A). The substitution of hydrogen (Φ -1.82_H₂-S) leads
318 to a shift of the temperature profile towards the burner surface, while the addition procedure
319 (Φ -1.82_H₂-A) does not cause any shift. In both approaches, the maximum temperature is
320 almost similar for the three flames, indicating an insignificant influence of the added H₂ on

321 this flame parameter. Indeed, the maximum temperature of the Φ -1.82_H₂-S and Φ -1.82_H₂-
322 A flames only differs from the reference flame by about 20 K. The temperature is almost
323 identical in the post flame zone of the three studied flames. The adiabatic temperature
324 calculated using GASEQ program [42] confirms the weak impact of H₂ on the flame
325 temperature profiles as shown in Table 1.

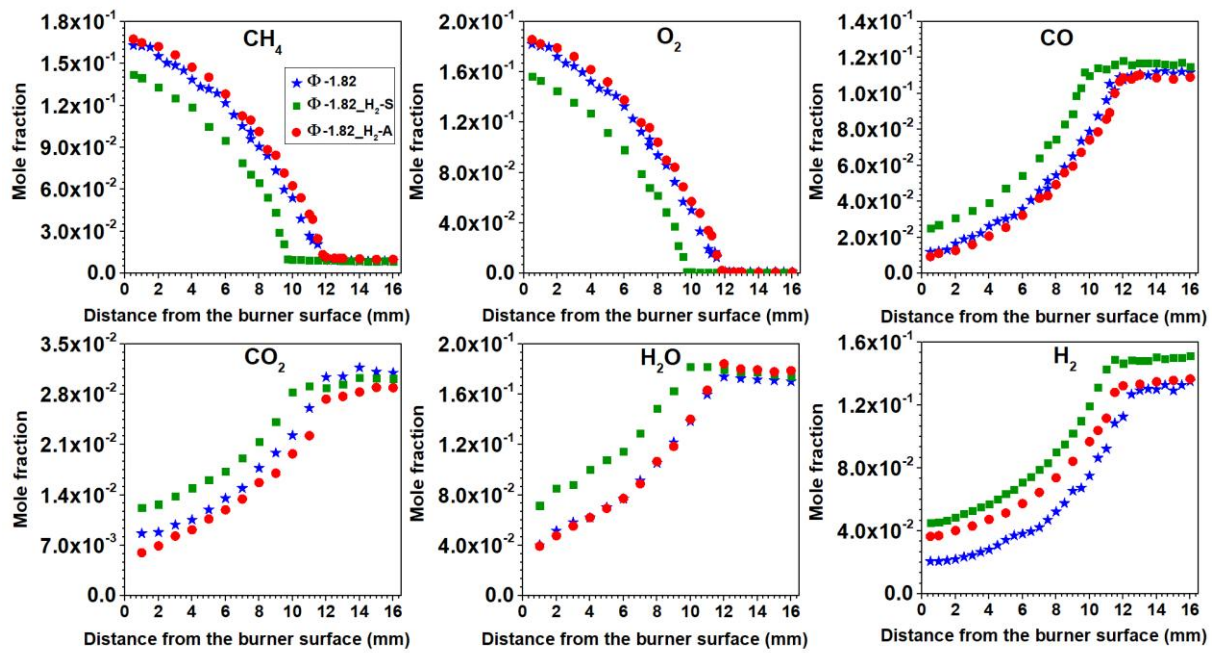


326

327 **Fig. 1.** Impact of hydrogen on flame temperature profiles. Φ -1.82: CH₄ flame; Φ -1.82_H₂-S: CH₄
328 substituted-H₂ flame; Φ -1.82_H₂-A: CH₄ added-H₂ flame (see Table 1 for the flame conditions).

329 3.2. Impact of hydrogen on major species (reactants and combustion products)

330 Figure 2 presents the mole fraction profiles as a function of the distance from the burner
331 surface of the main species including reactants (fuel, O₂) and final products (CO, CO₂, H₂,
332 H₂O) for the three studied flames.



333
 334 **Fig. 2.** Mole fraction profiles of reactants (fuel, O_2) and major products (CO , CO_2 , H_2 , H_2O) as a
 335 function of the distance from the burner surface, obtained in the three studied flames.

336
 337 **As observed for** the temperature profiles **reported** above, the H_2 substitution ($\Phi-1.82_{\text{H}_2\text{-S}}$)
 338 systematically shifts the profiles of the major species around 2 mm closer to the burner
 339 surface while the H_2 addition ($\Phi-1.82_{\text{H}_2\text{-A}}$) does not significantly modify the flame position.
 340 This shift can be attributed to the laminar flame speed increase in the case of H_2 substitution
 341 ($\Phi-1.82_{\text{H}_2\text{-S}}$). Indeed, according to our calculations carried out for the studied conditions
 342 using the GRI mechanism [57], the laminar flame speed of the flame $\Phi-1.82_{\text{H}_2\text{-S}}$ has been
 343 determined around 9.50 cm s^{-1} . **This value is actually** slightly higher **than the flame speed**
 344 **determined** for the reference flame speed (8.79 cm s^{-1}) **which is very close to the calculated**
 345 **flame speed of the** $\Phi-1.82_{\text{H}_2\text{-A}}$ **flame** (8.82 cm s^{-1}). As expected, the consumption rate of
 346 CH_4 does not nearly evolve anymore beyond 10 mm in the flame $\Phi-1.82_{\text{H}_2\text{-S}}$ and **beyond** 12
 347 mm **for** the two other flames, while O_2 is completely consumed above these distances. Thus,
 348 the reaction zone in which the fuel gradually decomposes and the combustion intermediates
 349 actively react with each other is located before these distances. The post-flame zone starts just

350 after the reaction zone where the final products (CO, CO₂, H₂, H₂O) become the dominant
351 species in this region. The formation of CO, CO₂, H₂ and H₂O is consistent with the
352 consumption of the fuel and O₂. Indeed, mole fractions of CO, CO₂, H₂ and H₂O expectedly
353 increase in the reaction zone until maximum values reached in the post-flame zone. The
354 slightly higher values of the mole fractions of these products in the reaction zone of the flame
355 Φ -1.82_H₂-S in comparison with the other flames, are explained by the slight shift of the
356 flame front closer to the burner surface. However, the impact of this shift only induces minor
357 changes (within 5%) of the mole fractions of CO, CO₂, and H₂O in the post-flame zone
358 between the different flames.

359

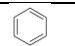
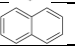
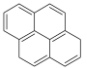
360 3.3. Impact of hydrogen on soot precursors

361 Hydrocarbon species from C₂ to C₁₆ corresponding to molar masses ranging from 26 to
362 202 were identified and quantified with maximum mole fractions comprised between 10⁻²-10⁻⁸
363 and peak position located between 7.5 and 12.5 mm above the burner. The whole species we
364 detected in the three studied flames associated with their chemical structures, maximum mole
365 fractions and peak positions are reported in Table 2. It is to be noted that the sensitivity of the
366 experimental analysis method used for PAH measurements enabled the detection of these
367 species until very low concentrations estimated around the ppb level for pyrene.

368

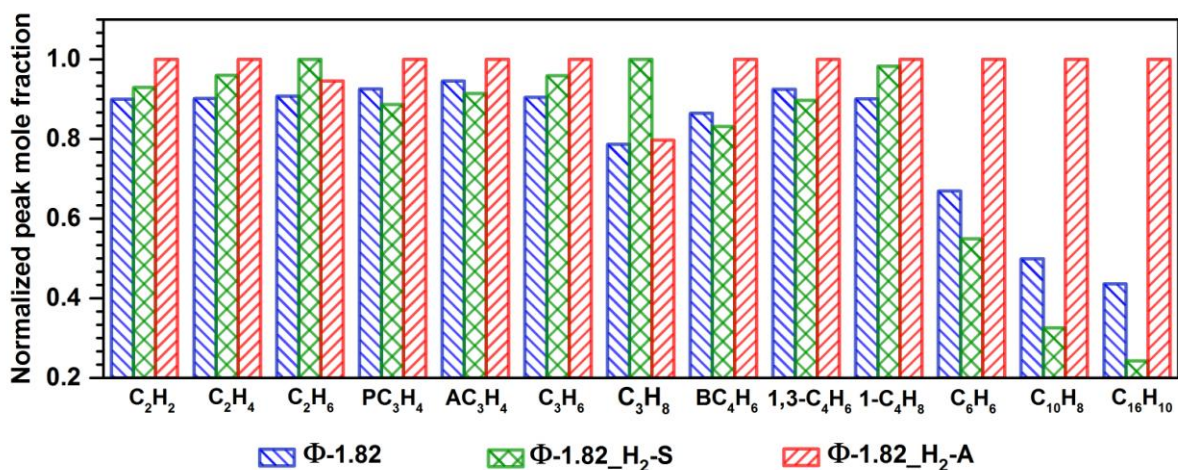
369

370 **Table 2.** Nomenclature, name, and structure of soot precursors in the studied flames together with
371 their measured maximum mole fractions x_{max} . DFBS: distance from the burner surface at x_{max} (mm).

Nomenclature	Name	Structure	Flame Φ -1.82		Flame Φ -1.82_H ₂ -S		Flame Φ -1.82_H ₂ -A	
			x_{max}	DFBS (mm)	x_{max}	DFBS (mm)	x_{max}	DFBS (mm)
C ₂ H ₆	Ethane	H ₃ C—CH ₃	6.62×10^{-4}	9.5	7.30×10^{-4}	7.5	6.90×10^{-4}	10.0
C ₂ H ₄	Ethylene	H ₂ C=CH ₂	1.57×10^{-3}	10.0	1.67×10^{-3}	7.5	1.74×10^{-3}	10.0
C ₂ H ₂	Acetylene	HC≡CH	1.17×10^{-2}	11.8	1.21×10^{-2}	9.7	1.30×10^{-2}	11.8
C ₃ H ₈	Propane	H ₃ C—CH ₂ —CH ₃	1.31×10^{-5}	11.2	1.66×10^{-5}	9.2	1.32×10^{-5}	11.5
C ₃ H ₆	Propene	H ₂ C=CH—CH ₃	2.21×10^{-5}	8.5	2.35×10^{-5}	7.5	2.45×10^{-5}	9.0
AC ₃ H ₄	Allene	H ₂ C=C=CH ₂	4.66×10^{-5}	11.2	4.50×10^{-5}	9.5	4.93×10^{-5}	11.5
PC ₃ H ₄	Propyne	HC≡C—CH ₃	1.11×10^{-4}	11.4	1.07×10^{-4}	9.5	1.20×10^{-4}	11.5
1-C ₄ H ₈	1-Butene	H ₃ C—CH ₂ —CH=CH ₂	3.00×10^{-6}	11.5	3.28×10^{-6}	9.2	3.34×10^{-6}	11.5
1,3-C ₄ H ₆	1,3-Butadiene	H ₂ C=CH—CH=CH ₂	6.74×10^{-6}	10.0	6.54×10^{-6}	7.5	7.29×10^{-6}	10.5
BC ₄ H ₆	1-Butyne	H ₃ C—CH ₂ —C≡CH	1.94×10^{-5}	11.5	1.87×10^{-5}	9.5	2.25×10^{-5}	11.8
C ₆ H ₆	Benzene		2.10×10^{-5}	11.4	1.72×10^{-5}	9.0	3.13×10^{-5}	11.8
C ₁₀ H ₈	Naphthalene		1.54×10^{-6}	11.5	1.01×10^{-6}	9.0	3.09×10^{-6}	11.5
C ₁₆ H ₁₀	Pyrene		3.97×10^{-8}	12.0	2.21×10^{-8}	9.5	9.10×10^{-8}	12.5

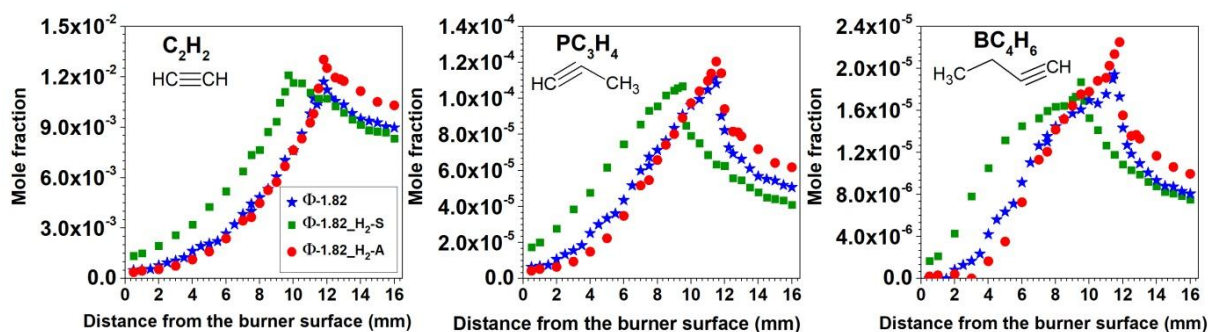
372

373 The impact of hydrogen on the formation of the measured species can be clearer appreciated
374 in Fig. 3 where we have reported the normalized maximum mole fractions, species by species,
375 measured in the three flames. As can be seen in this figure, the introduction of H₂ either by
376 addition or substitution, does not significantly influence the maximum mole fractions of the
377 measured aliphatic species. By contrast, it strongly impacts the peak mole fractions of the
378 measured aromatic species (benzene, naphthalene and pyrene), indicating a strong interaction
379 of H₂ chemistry with the formation of these aromatic species. This point will be discussed in
380 detail in the following.



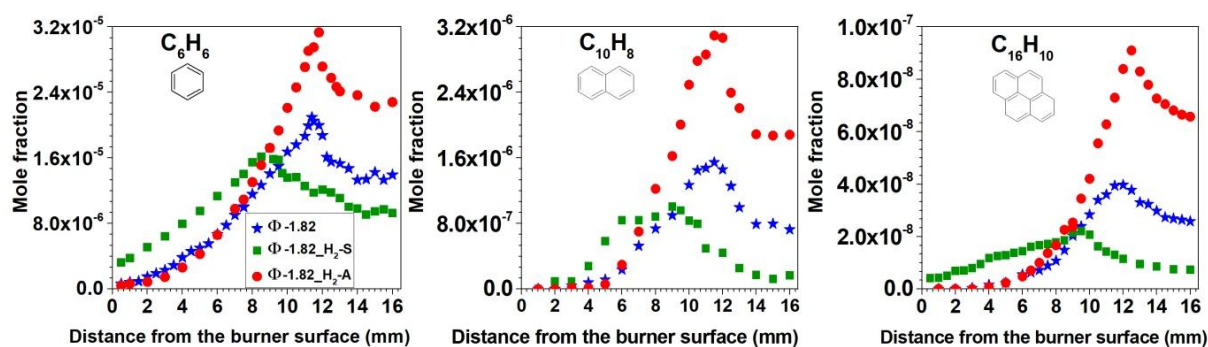
381
 382 **Fig. 3.** Graphical summary of the normalized maximum mole fractions of the soot precursors
 383 measured in the three studied flames. Normalization has been performed, species by species, regarding
 384 to the highest mole fraction value measured in the three flames.

385
 386 Selected mole fraction profiles of aliphatic and aromatic species measured in the three
 387 flames as a function of the distance from the burner surface are presented in Figs. 4 and 5.
 388 Figure 4 presents the mole fraction profiles of acetylene (C₂H₂), propyne (PC₃H₄) and 1-
 389 butyne (BC₄H₆) which are the most abundant species in their corresponding aliphatic group,
 390 i.e. characterized by a same carbon number. The mole fraction profiles of other aliphatic
 391 species are also available in SM1 (Fig. S7). From this figure, we note that the profiles of the
 392 species measured in the flame $\Phi-1.82_{H_2-S}$ are systematically shifted towards the burner
 393 surface, consistently with the fuel consumption behavior. However, the introduction of H₂
 394 highlights no significant effect on the shape of the profile and the maximum mole fraction as
 395 mentioned earlier. In the present study, only 10% H₂ compared to the fuel was introduced in
 396 the flame in order to limit its impact on the temperature profile and allows thus to
 397 “selectively” investigate the influence of H₂ on the **involved** species in the formation of soot
 398 particles.



399
400 **Fig. 4.** Mole fraction profiles of selected aliphatic species considered as soot precursors: acetylene,
401 propyne and 1-butyne obtained in the three studied flames.

402

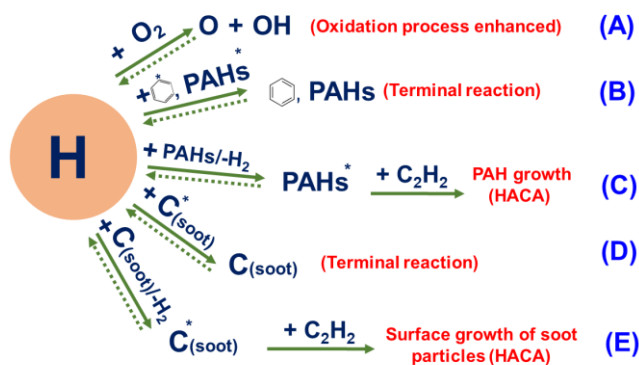


403
404 **Fig. 5.** Mole fraction profiles of benzene, naphthalene and pyrene obtained in the three studied flames.

405

406 Figure 5 presents the measured mole fraction profiles of benzene (C_6H_6), naphthalene
407 ($C_{10}H_8$), and pyrene ($C_{16}H_{10}$) which are aromatic species considered as important soot
408 precursors. As can be in this figure, the mole fraction profiles of these species are
409 significantly impacted by H_2 introduction. Moreover, these data show that the impact of H_2
410 depends on the molar mass of the aromatic compounds. The larger the size of the PAHs, the
411 greater the H_2 effect. It is important to note that the H_2 substitution ($\Phi-1.82_{H_2-S}$) presents an
412 inhibitory effect (20-50%) on the formation of benzene, naphthalene, and pyrene while the H_2
413 addition ($\Phi-1.82_{H_2-A}$) clearly promotes the formation of these aromatics (30-60%). To
414 explain such antagonistic effects, Fig. 6 presents possible competitive processes that share H
415 atoms as reactant. In flame conditions, H_2 can be converted to H atoms mainly by
416 $H_2+OH\rightarrow H+H_2O$ and $H_2+O\rightarrow H+OH$. The reaction $H_2+M\rightarrow H+H+M$ can also contribute to

417 this conversion in the post flame region. As can be seen from Fig. 6, the branching reaction
 418 (path A) competes with the benzene/PAH accumulation process (path B) and the PAH growth
 419 processes (path C). Paths D and E are related to soot particles and will be discussed in the
 420 next section.



421
 422 **Fig. 6.** Possible chemical paths characterizing the kinetic impact of hydrogen atoms in sooting flames.
 423 Species written with a star are radicals.

424
 425 We have shown that H atoms reinforced by the presence of H₂ in the case of substitution
 426 essentially serve the reaction (A). This leads to an increase of the laminar flame speed. In
 427 other words, H atoms are mainly converted to O and OH radicals under these conditions,
 428 resulting in accelerated oxidation processes of aromatic species and in a decrease of H atoms
 429 available for processes (B) and (C). These two points explain the decrease of aromatic species
 430 mole fraction analyzed under these conditions. In the case of the addition of hydrogen, the
 431 reaction (A) is not favored. This is confirmed by the flame front position and by the calculated
 432 laminar flame speed of both flames which are similar as reported in Table 1. Thus, H atoms
 433 from hydrogen addition sources would benefit primarily for processes (B) and (C). These
 434 processes naturally promote a greater formation of benzene and PAHs, giving a soot precursor
 435 promoting role to hydrogen under these conditions.

436 **Regarding the well-known and commonly used HACA mechanism, the growth process of**
 437 **PAHs is based** on an overall consecutive reaction sequence that begins from the first aromatic

438 ring. This growth process requires acetylene and numerous H-abstraction reactions from
439 PAHs mainly by H atoms. Therefore, in both cases (substitution or addition) the main factors
440 that could explain the important differences regarding the PAHs formation might be the
441 temperature, concentration of H atoms, benzene and acetylene. The analysis of our
442 experimental data allows us to exclude the effect of temperature and acetylene concentration.
443 The effect of H₂ is almost negligible on these two parameters. On the other hand, the
444 recombination of H and phenyl radicals (B) takes a very important role in aromatic species
445 formation in the post flame region as shown in our previous work [58]. The balance of power
446 between A and B processes can be considered at the origin of the experimental PAH
447 observations under the different conditions of the present investigation. Given the high
448 endothermicity of the H elimination from benzene reaction, the B process works in favor of
449 the first aromatic cycle formation. This reaction is very sensitive to the temperature and also
450 to the concentration of H atoms. For example, in the case of H₂ addition, the cumulative effect
451 of the temperature decrease and H concentration increase promotes the recombination
452 reaction of H with the phenyl radicals. Temperature profiles measured in both flames are
453 substantially identical. So, we can conclude that the observed different impacts on the PAH
454 formation mainly comes from H atoms. Note that the effect is also noticeable on benzene and
455 therefore on PAH mole fraction from 9 mm. Before this position, the impact is limited
456 because reaction B is not dominant in this zone. Outside the soot area, the main reactions
457 regarding the benzene formation are the self-propargyl recombination and the addition of
458 acetylene on butadienyl radicals.

459 In summary, the promoting effect (addition) or inhibiting effect (substitution) of hydrogen
460 on PAH formation can be explained by a strong competition between the high temperature
461 branching reaction (A) and the recombination of phenyl radicals with H atoms process (B).
462 The decrease (substitution) or increase (addition) of benzene mole fraction mechanically

463 results in a reduction or increase in PAHs given the **crucial role** of benzene at the beginning of
464 the HACA sequence governing the growth of PAHs. As the sequence is consecutive, the
465 weaker is the mole fraction of aromatic compound in the reference flame, the stronger the
466 effect of a small variation in benzene is. The effect is therefore logically more important on
467 pyrene than on naphthalene in all studied flames.

468 It is important to specify here that the effect of H₂ in the case of substitution is clearly
469 chemical and that our results exclude a dilution effect. Indeed, the substitution of H₂ in this
470 flame by an equivalent amount of helium does not lead to any variations of the measured
471 species mole fraction profiles. This point is highlighted in Fig. S8 where we report the mole
472 fraction profiles of benzene and its aliphatic precursors measured in the CH₄ flame with added
473 He compared to the CH₄ reference flame. In the case of addition (Φ -1.82_H₂-A), the
474 replacement of H₂ by an equivalent amount of helium could not be performed in this flame
475 because of the flame instability generated by the higher dilution. Therefore, it has not been
476 possible to check the dilution effect on the mole fraction profiles of the measured species
477 according to this approach (He addition) in the flame Φ -1.82_H₂-A. However, the difference
478 in the dilution ratio between the reference flame Φ -1.82 and the flame Φ -1.82_H₂-A is very
479 small (<2%), suggesting that the H₂ dilution effect **is certainly** negligible. Therefore, it seems
480 reasonable to consider that the differences observed between mole fraction profiles measured
481 in the reference flame Φ -1.82 and the flame Φ -1.82_H₂-A result from chemical effects due to
482 H₂ addition.

483

484 **3.4. Impact of hydrogen on the formation of soot particles**

485 **3.4.1. Determination of the nucleation flame conditions by LII**

486 The LII technique is a powerful and sensitive technique to study soot particles in flames.
487 Details of the method can be found in numerous papers [56,59–62]. Briefly, the measured LII

488 signal, corresponding to the incandescent emission coming from the heated soot particles by a
489 laser pulse, can be expressed according to the following expression:

$$490 \quad S_{LII}(\lambda_{em}, T_p(t)) = 48 \cdot E(m) \frac{\pi^2 \cdot h \cdot c^2}{\lambda_{em}^6} \cdot \left[\exp\left(\frac{h \cdot c}{\lambda_{em} \cdot k_b \cdot T_p(t)}\right) - 1 \right]^{-1} \cdot f_v \quad eq.1$$

491

492 where $E(m)$ is the absorption function of the particles, T_p the temperature of the heated soot
493 by the laser pulse, c the speed of light, λ_{em} the emission wavelength, k_b the Boltzmann
494 constant, h the Planck constant and f_v the soot volume fraction. This last quantity can be
495 further defined as:

$$496 \quad f_v = \frac{4}{3} \cdot \pi \cdot r_p^3 \cdot N_p \quad eq.2$$

497 where N_p and r_p are respectively the number by unit volume and radius of the soot particles.

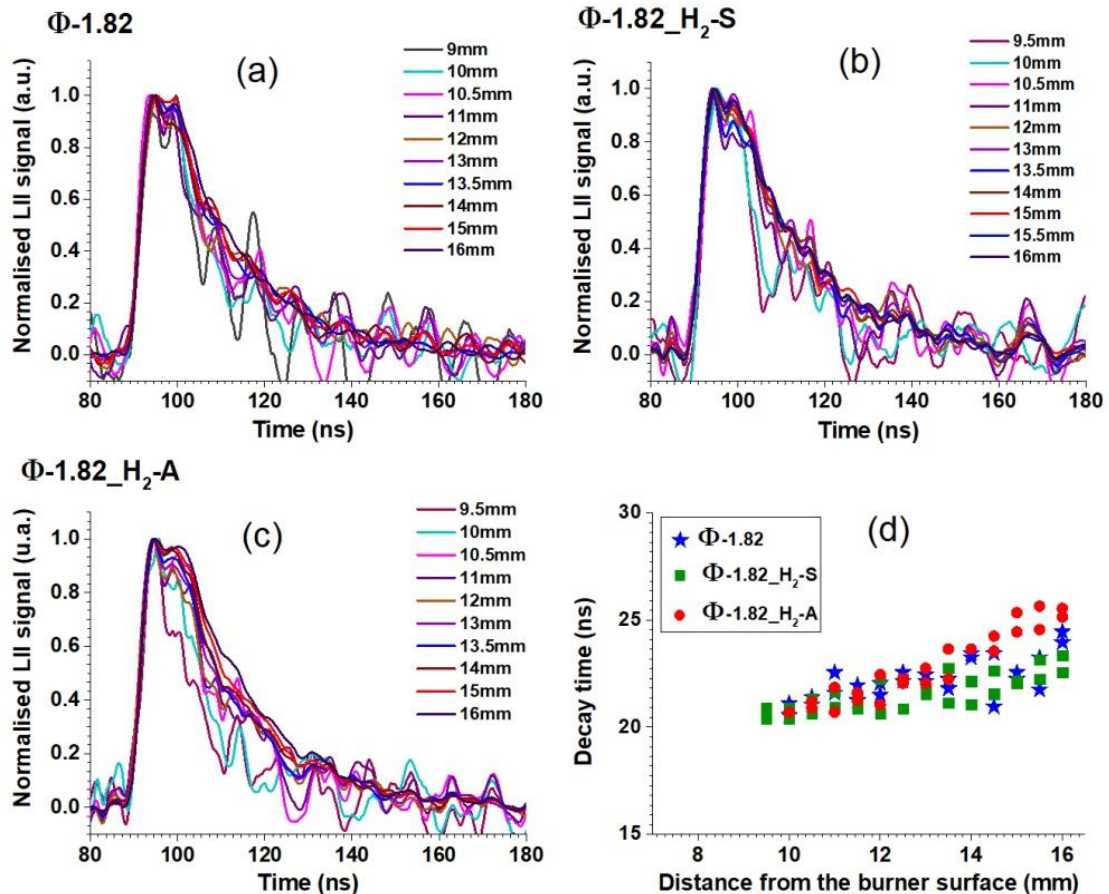
498 The LII signal is therefore directly related to the size of the generated soot particles and can
499 be used adequately to determine the conditions of the “nucleation” flame, characterized by an
500 invariance of the temporal decay of the LII signals all along the flame height. Hence, the
501 equivalence ratio enabling the generation of the “nucleation flame” in this work has been
502 obtained by following the evolution of the LII temporal decays along the flame height
503 according to a procedure **already** described in details elsewhere [44,45]. The relationship
504 between the LII temporal decay and the soot size distribution is quite complex [60,63] and
505 requires the use of specific models to interpret the LII signals in terms of primary particle
506 diameter. However, it has been established that the temporal LII decay time is correlated to
507 the diameter of soot particles [60,63] and that the variation of this decay time **might be used to**
508 **characterize** the variation of the soot diameter. The longer the decay time the larger the soot
509 particle diameter. Here, we only focus on the characterization of the influence of H_2 as a fuel
510 additive on the relative size of the soot diameter. The determination of the absolute value of
511 the soot particle diameters **which can be obtained** by modelling the LII signals, although being

512 an interesting topic, is clearly beyond the scope of this paper and will be dealt in a future
513 dedicated work.

514 We took here benefit of this technique to determine the conditions of the nucleation flames
515 and to examine the influence of added H₂ on the soot formation. These flame conditions were
516 obtained by adjusting the flow rate of the reactants so that we do not observe any growth of
517 the temporal LII decay time all along the flame height, meaning that the size of the soot
518 particles remain constant regardless the height above the burner. By this way, we defined the
519 equivalence ratio $\Phi=1.82$ as the condition characterizing the reference “nucleation flame”
520 (denoted flame $\Phi=1.82$, see flame conditions in Table 1). The corresponding LII signals
521 according the height above the burner are reported in Fig. 7a, while the determined decay
522 times (corresponding to the time measured at 1/e from the maximum intensity) of these
523 temporal signals are reported in Fig. 7d. Similarly, the temporal LII signals measured in the
524 two flames with added hydrogen, $\Phi=1.82_{H_2-S}$ and $\Phi=1.82_{H_2-A}$, are respectively reported in
525 Fig. 7b, c. The corresponding LII decay times for these flames are also reported in Fig. 7d. As
526 can be seen, the introduction of a small amount of H₂ in the reference flame does not induce
527 any significant variations the evolution of the LII decays, meaning that the propensity of soot
528 formation of the flames $\Phi=1.82_{H_2-S}$ and $\Phi=1.82_{H_2-A}$ are close to the one of the “nucleation
529 flame” conditions. This statement is corroborated by the data reported in Fig. 7d,
530 corresponding to the evolution of the LII decay times for the three studied flames. These data
531 highlight a quite constant value of the decay times according to the flame height in the three
532 flames, excepted in the post-flame zone between 14 and 16 mm where we note a slight
533 increase. These data therefore confirm the absence or very weak efficiency of soot growth
534 processes in these three flames, meaning that nucleation is clearly the major process
535 implicated in these flames. It moreover confirms that the small amounts, provided by
536 substitution or addition of H₂ to the reference flame, do not significantly influence the size of

537 the soot particles in the early soot formation zone. This property therefore provides a useful
 538 opportunity to inspect further the role of the introduced H₂ on the formation mechanism of
 539 nascent soot particles, as discussed in the next sections.

540



541
 542 **Fig. 7.** LII temporal signals measured at different distances from the burner surface in the three
 543 studied flames: (a) CH₄ flame ($\Phi-1.82$), (b) CH₄ substituted-H₂ flame ($\Phi-1.82_{H_2-S}$), (c) CH₄ added-
 544 H₂ flame ($\Phi-1.82_{H_2-A}$). For clarity, the peak of LII signals have been normalized to 1. Laser fluence
 545 was set at 0.415 J cm⁻². (d) LII decay-times measured at 1/e of the LII signal as a function of the
 546 distance from the burner surface.

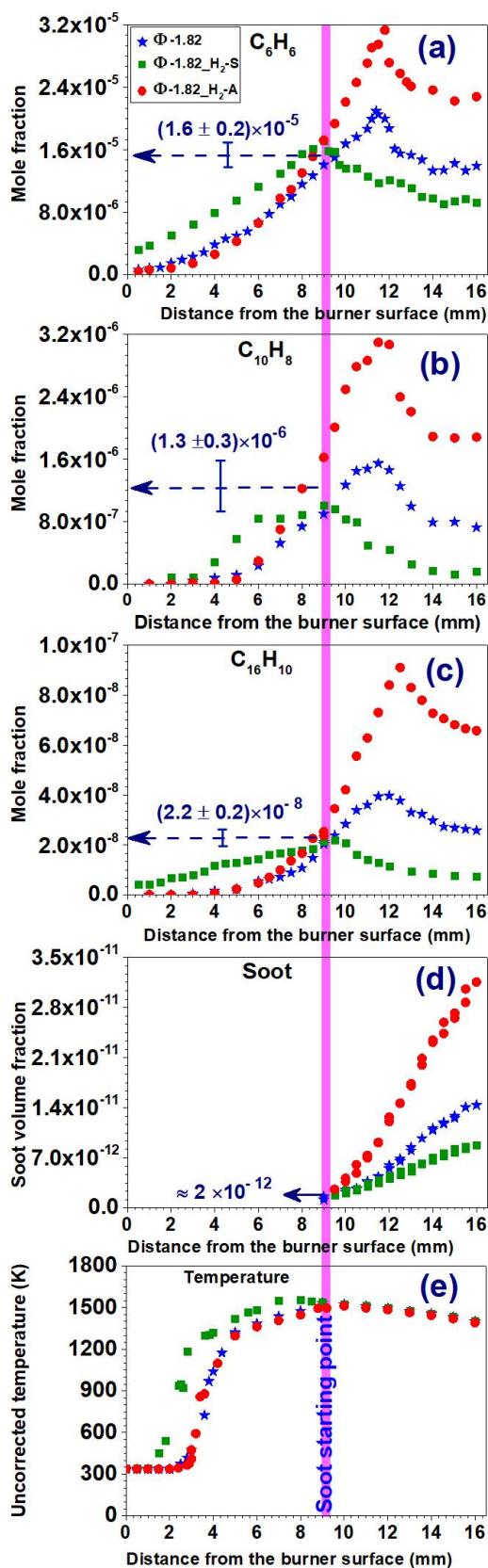
547

548 3.4.2. Impact of hydrogen on the appearance of nascent soot particles

549 Although the mechanism of formation of nascent soot particles from PAHs precursors is still
 550 discussed in the community, a large number of studies [43,47,64–69] mentioned that
 551 moderate sized PAHs as pyrene could play an important role in the nucleation process. More

552 specifically, the formation of dimers of such PAHs has been suggested as a potential key step
553 allowing the formation of nascent soot particles [47,66–73]. However, because of the weak
554 energy of the Van der Waals bonds characterizing dimers of PAHs, especially at flame
555 temperature [74,75], this hypothesis has often been considered as a numerical tool for kinetic
556 modelling rather than a real physical process actually **involved** in sooting flames. In that
557 context, Kholghy *et al.* [72] recently suggested a model for the soot nucleation relying on the
558 reversibility of the nucleation process [71,75] associated to the formation of homo and
559 heterogeneous dimers of low molecular weight, stabilized by the formation of a covalent
560 carbon-carbon bond between the two PAHs constituted the dimer. The formation of bonded
561 dimers of moderate-sized PAHs, either by formation of direct covalent bonds or aliphatic
562 bridges, is a current hot topic in the combustion community and has been the subject of
563 different recent experimental and modeling works [68,72,73,76–81]. From these papers, it
564 appears that more and more studies support the idea of a crucial implication of moderate-sized
565 PAHs in the nucleation step leading the formation of the very first particles in flames.

566 Hence, to further explore this hypothesis and the potential implication of hydrogen in this
567 mechanism, we studied the formation of the very first soot particles formed in our three
568 flames. Figure 8a-c gather the experimental profiles of aromatics (benzene, naphthalene and
569 pyrene) expected to be key species for soot formation. We also report in Fig. 8d the
570 corresponding soot volume fraction profiles measured in each flame. Because of its
571 importance in the analysis of the soot formation, the temperature profiles of the three flames
572 are also added in this figure (Fig. 8e).



573

574 **Fig. 8.** Profiles of benzene, naphthalene and pyrene mole fraction, soot volume fraction and
 575 temperature obtained in the studied flames. The line at 9 mm is drawn to guide the eye regarding the
 576 starting point of soot formation.

577 Several important observations can be drawn from these results. The **first one** concerns the
578 similar trends (increase or decrease) of the PAHs and soot particles maximum values upon H₂
579 addition or substitution. These data notably show that the formation of soot particles and
580 PAHs are significantly promoted in the flame Φ -1.82_H₂-A while they are strongly inhibited
581 in the flame Φ -1.82_H₂-S (Fig. 8d). Furthermore, the H₂ substitution or addition affects very
582 strongly the PAHs mole fraction in the zone of soot particles formation (Fig. 8a-c). Although
583 this might appear as an expected result, it is important to remind here that we did not observe
584 in these conditions such strong effect on the measured aliphatic precursors as acetylene,
585 propyne, and allene. This experimental observation confirms that aromatic compounds are,
586 much more than aliphatic ones, crucial species in the nucleation process. The role of each
587 aromatic component in the soot nucleation process will be further examined in the next
588 section (Section 3.4.3).

589 Besides the chemical pathways involving PAHs, a direct influence of the H₂ introduction
590 via the processes (D) and (E) on the concentration of soot particles is not excluded (Fig. 6)
591 although these processes could be less predominant in the early soot nucleation zone [47]. The
592 temperature profiles (Fig. 8e) are quite similar for the three studied flames as discussed
593 earlier. This information is crucial for our further analysis as it guarantees that the differences
594 observed between the soot volume fraction profiles of the three flames are only due to
595 chemical effects related to the introduction of H₂.

596 The **second observation** which can be made from these data, is the existence of an
597 intercrossing point of the aromatic mole fraction profiles, identified by a pink line in Fig. 8a-
598 c, at a height around 9 mm above the burner, corresponding to the first appearance of the very
599 first particles in each flame. Hence, although H₂ strongly impacts the flame position and the
600 magnitude of the PAH/soot profiles (see Fig. 8a-d), it has no notable influence on the starting
601 point of soot particles profiles. Besides, not only the first soot particles begin to appear at the

602 same height in all these flames but also the corresponding mole fractions of benzene,
603 naphthalene and pyrene measured at this height display very similar values in the three
604 flames, around 1.6×10^{-5} (16 ppm), 1.3×10^{-6} (1.3 ppm), and 2.2×10^{-8} (22 ppb) for benzene,
605 naphthalene and pyrene respectively. Moreover, it is remarkable that the corresponding
606 volume fraction of soot particles determined at 9 mm also highlight a constant value close to
607 $\sim 2 \times 10^{-12}$ (~ 2 ppt) in each flame. We precise here that the sensitivity of the LII technique used
608 to carry out these measurements has been demonstrated to be at least 10 times better (around
609 0.1 ppt) in a previous work [43]. Hence, these data might suggest that the start of the soot
610 formation process might be dependent on specific minimum *concentration “thresholds” of*
611 *aromatic species*, above only which the nucleation process could take place.

612 This idea can be rather corroborated by previous measurements of pyrene mole fractions
613 and soot volume fractions made in a methane nucleation flame at low pressure (200 Torr)
614 [43], the profiles of which being reported in Fig. S9. We added on this figure the
615 corresponding species profiles measured in the current atmospheric nucleation flames for
616 comparison. This figure shows that the mole fraction of pyrene measured in the low pressure
617 flame [43] at the very beginning of the soot formation zone reaches a quite similar mole
618 fraction value (~ 22 ppb) as the one measured here in the atmospheric flames (see Fig. S9).

619 Much experiments are obviously required to state about this hypothesis of minimum
620 concentration thresholds of aromatics which may be required to enable the soot particle
621 inception to take place. Indeed, although other studies addressed to flames, highlighted
622 properties close to nucleation flames properties exist in the literature, *e.g.* [44,82], no
623 quantitative profile of aromatics simultaneously measured with soot particles was reported in
624 these works, therefore precluding any further comparisons.

625

626 3.4.3. Impact of hydrogen on the soot nucleation rate

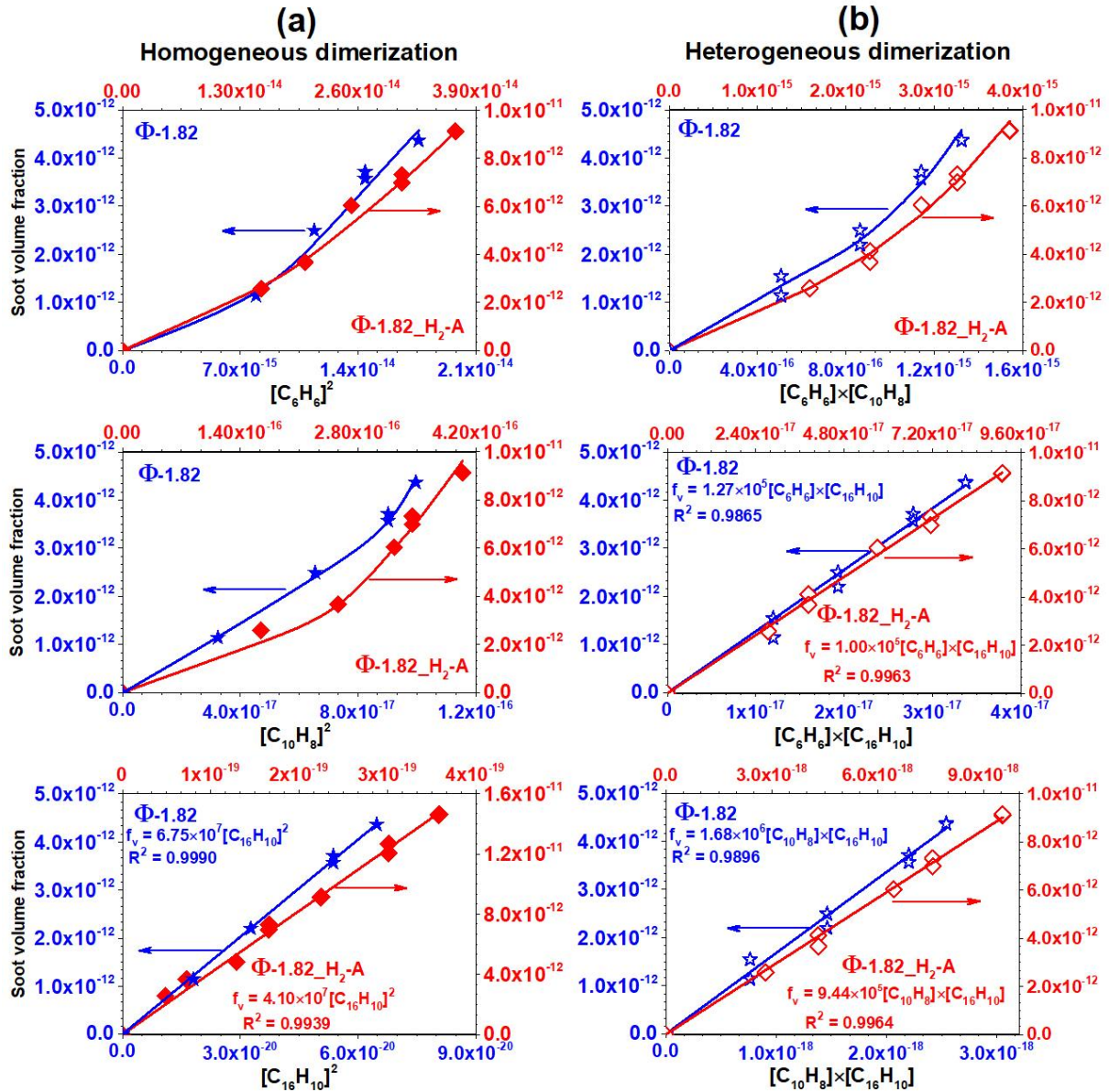
627 To complete the above discussion about the likely dependence of the soot starting point to
628 concentration thresholds of PAHs, we attempt in the present section to discuss the role of the
629 measured individual PAHs on the formation process of the “first” soot particles and the
630 influence of H₂ addition in that context.

631 As discussed above, a large number of studies and recent theories [43,72,73,75,77]
632 suggest that the formation of the first soot particles comes from the dimerization process of
633 moderate-sized PAHs. From an experimental point of view, Mercier *et al* [73] recently
634 highlighted that the laser induced fluorescence signals emitted in the visible range (450-750
635 nm), commonly observed in the inception region of sooting flames, might very likely
636 characterize the formation of dimers of moderate-sized PAH. Such hypothesis should
637 therefore imply some kinds of proportional relationships between the nascent soot particles
638 number N_p and the concentration of two PAHs, related to the dimer formation.

639 The net rate of soot formation normally results from the sum of the rates of many processes
640 such as soot nucleation, soot oxidation, soot growth by PAH condensation on soot surface,
641 chemical soot surface growth (HACA mechanism) and soot particle coagulation. Hence, in
642 standard sooting flames, the complexity of this expression does not allow to establish an
643 immediate correlation between gaseous soot precursors and **the formed** soot particles. The
644 complexity is even greater if one considers the reversibility of the previous processes. The
645 great advantage of the nucleation flame used in the present study is that this kind of flames
646 allows to minimize many of these processes. In this case, the expression of the net soot
647 formation rate is simplified due to the establishment of a balance between the global soot
648 growth rate and the soot oxidation rate [43]. However, as highlighted by the LII results (Fig.
649 7), this property (balance between the soot growth and oxidation rates) cannot be considered
650 as fully achieved along the flame height, even in a nucleation flame. We indeed showed above

651 that the soot growth process is not completely inactive in our three nucleation flames, mostly
652 in the zone after the peak of PAHs. So, in order to accurately characterize the reactive species
653 and chemical reactions involved in the nucleation process, it is necessary to specifically
654 consider the soot starting zone where only the nucleation process is activated. To this aim, we
655 have chosen the reaction zone located before the peak of the aromatic species for the analysis
656 of the suggested hypothesis related to the soot formation.

657 As discussed above, the number of particles N_p is related to the soot volume fraction f_v
658 according to the eq. 2. In the reaction zone located before the peak of the aromatic species of
659 the nucleation flame, the value of r_p , corresponding to the soot radius, remains always
660 constant in this height range of the studied flames. Hence the number of particles N_p is in this
661 case directly proportional the values of f_v measured in this work. In order to appreciate the
662 nature of the aromatic precursors involved in the nucleation process, we have reported the
663 evolution of f_v according to the square of the corresponding concentration of aromatics
664 species (homogeneous dimerization) and the evolution of f_v according to the product of the
665 concentrations of two different PAHs (heterogeneous dimerization). These data are presented
666 in Fig. 9 for the reference methane flame (Φ -1.82) and methane H_2 -added flame (Φ -1.82- H_2 -
667 A). The presented concentration values of benzene, naphthalene and pyrene have been
668 determined from their measured mole fraction profiles and the corresponding temperature
669 profiles.



670
 671 **Fig. 9.** Influence of H₂ on the relationship between the soot volume fraction and the squared
 672 concentration of benzene, naphthalene, and pyrene ($[C_6H_6]^2$, $[C_{10}H_8]^2$, and $[C_{16}H_{10}]^2$) respectively (a)
 673 and the product of the concentrations of two different PAHs ($[C_6H_6] \times [C_{10}H_8]$, $[C_6H_6] \times [C_{16}H_{10}]$,
 674 $[C_{10}H_8] \times [C_{16}H_{10}]$) (b) in the soot inception zone of flames Φ-1.82 and Φ-1.82_H₂-A. Flame Φ-1.82:
 675 left and bottom axes. Flame Φ-1.82_H₂-A: right and top axes. Symbols: experiment. Lines in bottom
 676 panel of (a), in middle and bottom panels of (b): linear fit. Lines in other panels: mean curve to guide
 677 the eye.

678
 679 Figure 9a clearly highlights a **direct relationship of proportionality** between pyrene
 680 squared concentration ($[C_{16}H_{10}]^2$) and soot volume fraction (f_v) characterized by a linear
 681 dependence of these two sets of data in both flames with and without H₂ addition. By contrast,

682 such linear relation is not observed in the case of benzene nor in the case of naphthalene
683 ($[C_6H_6]^2$, $[C_{10}H_8]^2$). The results therefore support this idea of dimerization of moderate sized
684 PAHs as a key step in the soot nucleation process discussed above. Obviously, pyrene might
685 not be the only one species this size implicated in the soot nucleation step. However, the
686 experimental evidence provided here highlights the pertinence of choosing this species in soot
687 models as a key species to represent the soot nucleation process according to a dimerization
688 process, *i.e.* a process depending on the pyrene-squared concentration [43,47,65,66,83].

689 Figure 9a also show that **H₂ addition** influences the slope of the regression line
690 characterizing the relationship between $[C_{16}H_{10}]^2$ and f_v . This slope is indeed slightly reduced
691 in the flame Φ -1.82_H₂-A in comparison with the flame Φ -1.82. This reduction therefore
692 denotes a lower formation rate of the nascent soot particles in the flame Φ -1.82_H₂-A,
693 although this flame has been shown to produce more soot than the reference flame (Fig. 8d).
694 The higher total amount of soot produced in the flame Φ -1.82_H₂-A can be easily justified by
695 the higher mole fractions of PAHs formed in this flame.

696 Assuming that the rate of all the other processes involved in the formation of nascent soot
697 (oxidation of soot, coagulation of nascent soot, condensation of PAHs on the surface of soot,
698 growth in size by chemical reactions of the HACA mechanism, etc.) are unchanged between
699 the flames, the observed reduction of the nucleation rate can be exclusively explained by the
700 effect of hydrogen. If, as suggested by our experimental data, dimerization of pyrene (or other
701 similar sized PAHs) are concerned by the nucleation process, such dimers of moderate-sized
702 PAHs have to be stabilized in order to survive at flame temperature and lead to soot particles.
703 One possibility of stabilization of these dimers would require, as suggested by recent works
704 discussed above, the formation of a chemical bond between the two PAHs constituted the
705 dimer after the physical dimerization (by van der Waals forces). Because this process must
706 release H or H₂, the reversed direction of the process could then be enhanced when adding H₂,

707 thus reducing the soot nucleation rate as observed for the flame Φ -1.82_H₂-A in comparison
708 with the reference flame. The present results therefore support this idea already introduced in
709 the soot formation mechanism developed by Khoghy *et al.* [72].

710 Finally, it is highly probable, as already said, that heterogeneous dimerization processes
711 implicated pyrene with other PAHs actively participate to the nucleation process. Such
712 mechanisms have notably been proposed in recent kinetic models [72]. This hypothesis has
713 also been considered according to our experimental data by considering different
714 combinations of aromatics to form dimers. These data, corresponding to the products of the
715 considered aromatic concentrations [C₆H₆] \times [C₁₀H₈], [C₆H₆] \times [C₁₆H₁₀], [C₁₀H₈] \times [C₁₆H₁₀] have
716 been reported in Fig 9b according the measured value of f_v in the two flames Φ -1.82 and
717 Φ -1.82_H₂-A. A linear relationship of proportionality is also observed only when pyrene
718 participates (Fig. 9b, middle and bottom panels). The data therefore strengthen the idea that
719 heterogeneous dimerization processes might play a crucial role, besides homogeneous
720 dimerization, in the soot nucleation process. Moreover, it reinforces the importance of pyrene
721 as a key species in the soot formation models to account for the soot nucleation process.

722

723 **4. Summary and Conclusion**

724 This paper reports new experimental data obtained in atmospheric “nucleation” flames of
725 methane with and without additional amounts of H₂ (~10% molar). Our results clearly
726 demonstrate the influence of H₂ as a fuel-additive on the formation of soot precursors and first
727 soot particles. These results notably show that the introduction of H₂ strongly influences the
728 concentration of aromatic species and soot, either increases or decreases, according to the
729 operating conditions (addition or substitution of H₂). By contrast, no significant modification
730 was observed regarding the mole fraction profiles of the aliphatic species we measured, even
731 though these species are usually considered as soot precursors as well.

732 Furthermore, these data also seem to suggest that the inception of the soot particle
733 formation might be controlled by specific concentrations of aromatic precursors, above which
734 the nucleation process can be initiated. This hypothesis is well supported by the
735 measurements of the aromatic concentrations at the very beginning of the soot profiles,
736 characterized by remarkable constant values in all studied flames. These values potentially
737 allowing **the inception of the soot formation process have been determined** around 16 ppm, 1
738 ppm and 22 ppb **respectively** for benzene, naphthalene and pyrene. Although much deeper
739 experiments are required to conclude about these hypothetical threshold values, they have
740 already been highlighted to be consistent with previous experiments carried out in a low-
741 pressure nucleation flame of methane. Such investigations will be the subject of future works
742 by examining whether the existence of these aromatic concentration thresholds are
743 independent of the flame operating conditions and nature of the fuel.

744 Finally, this work also demonstrates a linear relationship of proportionality between the
745 pyrene squared concentrations and soot volume fractions measured in the inception zone of
746 the soot particles, supporting therefore the hypothesis of pyrene dimerization to describe the
747 nucleation process in soot kinetic models. It is to be noted that the possibility of
748 heterogeneous dimerization of pyrene with benzene and naphthalene has also been checked.
749 Similar linear relationships with soot volume fraction have also been demonstrated in these
750 cases. These results therefore strongly suggest that dimerization, either according
751 homogenous or heterogeneous processes of moderate-sized PAHs, might be the key step
752 governing the soot nucleation process.

753 These reported data finally constitute a solid database to validate kinetic models of
754 PAHs/soot formation in CH₄/H₂ fuel mixtures. They pave the ways to future studies and
755 further comprehensive modeling analysis to elucidate the role of the identified key species
756 and associated reactions involved in the soot nucleation process.

758 **Acknowledgements**

759 This work was supported by the Agence Nationale de la Recherche through the LABEX
 760 CAPPa (ANR-11-LABX-0005), the Région Hauts-de-France, the Ministère de
 761 l'Enseignement Supérieur et de la Recherche (CPER Climibio) and the European Fund for
 762 Regional Economic Development.

763

764 **References**

- 765 [1] Zhang X, Zhang M, Zhang H, Jiang Z, Liu C, Cai W. A review on energy, environment
 766 and economic assessment in remanufacturing based on life cycle assessment method. *J*
 767 *Clean Prod* 2020;255:120160. <https://doi.org/10.1016/j.jclepro.2020.120160>.
- 768 [2] Johnsson F, Kjärstad J, Rootzén J. The threat to climate change mitigation posed by the
 769 abundance of fossil fuels. *Clim Policy* 2019;19:258–74.
 770 <https://doi.org/10.1080/14693062.2018.1483885>.
- 771 [3] Abdin Z, Zafaranloo A, Rafiee A, Mérida W, Lipiński W, Khalilpour KR. Hydrogen as
 772 an energy vector. *Renew Sustain Energy Rev* 2020;120:109620.
 773 <https://doi.org/10.1016/j.rser.2019.109620>.
- 774 [4] Nunes LJR, Causer TP, Ciolkosz D. Biomass for energy: A review on supply chain
 775 management models. *Renew Sustain Energy Rev* 2020;120:109658.
 776 <https://doi.org/10.1016/j.rser.2019.109658>.
- 777 [5] Abdel-Shafy HI, Mansour MSM. A review on polycyclic aromatic hydrocarbons:
 778 Source, environmental impact, effect on human health and remediation. *Egypt J Pet*
 779 2016;25:107–23. <https://doi.org/10.1016/j.ejpe.2015.03.011>.
- 780 [6] Ghorani-Azam A, Riahi-Zanjani B, Balali-Mood M. Effects of air pollution on human
 781 health and practical measures for prevention in Iran. *J Res Med Sci* 2016;21.
 782 <https://doi.org/10.4103/1735-1995.189646>.
- 783 [7] Lin R-H, Ye Z-Z, Wu B-D. A review of hydrogen station location models. *Int J*
 784 *Hydrogen Energy* 2020. <https://doi.org/10.1016/j.ijhydene.2019.12.035>.
- 785 [8] Shen X, Zhang C, Xiu G, Zhu H. Evolution of premixed stoichiometric hydrogen/air
 786 flame in a closed duct. *Energy* 2019;176:265–71.
 787 <https://doi.org/10.1016/j.energy.2019.03.193>.
- 788 [9] Xiao H, Duan Q, Sun J. Premixed flame propagation in hydrogen explosions. *Renew*
 789 *Sustain Energy Rev* 2018;81:1988–2001. <https://doi.org/10.1016/j.rser.2017.06.008>.
- 790 [10] Ma F, Wang Y, Liu H, Li Y, Wang J, Zhao S. Experimental study on thermal efficiency
 791 and emission characteristics of a lean burn hydrogen enriched natural gas engine. *Int J*
 792 *Hydrogen Energy* 2007;32:5067–75. <https://doi.org/10.1016/j.ijhydene.2007.07.048>.
- 793 [11] de Ferrières S, El Bakali A, Lefort B, Montero M, Pauwels JF. Experimental and
 794 numerical investigation of low-pressure laminar premixed synthetic natural gas/O₂/N₂
 795 and natural gas/H₂/O₂/N₂ flames. *Combust Flame* 2008;154:601–23.
 796 <https://doi.org/10.1016/j.combustflame.2008.04.018>.

- 797 [12] Anandarajah G, McDowall W, Ekins P. Decarbonising road transport with hydrogen and
798 electricity: Long term global technology learning scenarios. *Int J Hydrogen Energy*
799 2013;38:3419–32. <https://doi.org/10.1016/j.ijhydene.2012.12.110>.
- 800 [13] Jones DR, Al-Masry WA, Dunnill CW. Hydrogen-enriched natural gas as a domestic
801 fuel: an analysis based on flash-back and blow-off limits for domestic natural gas
802 appliances within the UK. *Sustain Energy Fuels* 2018;2:710–23.
803 <https://doi.org/10.1039/C7SE00598A>.
- 804 [14] Yangaz MU, Özdemir MR, Şener R. Combustion performance of hydrogen-enriched
805 fuels in a premixed burner. *Environ Technol* 2020;41:2–13.
806 <https://doi.org/10.1080/09593330.2019.1656676>.
- 807 [15] de Santoli L, Lo Basso G, Barati S, D'Ambra S, Fasolilli C. Seasonal energy and
808 environmental characterization of a micro gas turbine fueled with H2NG blends. *Energy*
809 2020;193:116678. <https://doi.org/10.1016/j.energy.2019.116678>.
- 810 [16] Shen X, Xiu G, Wu S. Experimental study on the explosion characteristics of
811 methane/air mixtures with hydrogen addition. *Appl Therm Eng* 2017;120:741–7.
812 <https://doi.org/10.1016/j.applthermaleng.2017.04.040>.
- 813 [17] Zhang C, Shen X, Wen JX, Xiu G. The behavior of methane/hydrogen/air premixed
814 flame in a closed channel with inhibition. *Fuel* 2020;265:116810.
815 <https://doi.org/10.1016/j.fuel.2019.116810>.
- 816 [18] Halter F, Chauveau C, Gökalp I. Characterization of the effects of hydrogen addition in
817 premixed methane/air flames. *Int J Hydrogen Energy* 2007;32:2585–92.
818 <https://doi.org/10.1016/j.ijhydene.2006.11.033>.
- 819 [19] Hawkes ER, Chen JH. Direct numerical simulation of hydrogen-enriched lean premixed
820 methane–air flames. *Combust Flame* 2004;138:242–58.
821 <https://doi.org/10.1016/j.combustflame.2004.04.010>.
- 822 [20] Hu E, Huang Z, Zheng J, Li Q, He J. Numerical study on laminar burning velocity and
823 NO formation of premixed methane–hydrogen–air flames. *Int J Hydrogen Energy*
824 2009;34:6545–57. <https://doi.org/10.1016/j.ijhydene.2009.05.080>.
- 825 [21] Kumar P, Mishra DP. Experimental investigation of laminar LPG–H2 jet diffusion
826 flame. *Int J Hydrogen Energy* 2008;33:225–31.
827 <https://doi.org/10.1016/j.ijhydene.2007.09.023>.
- 828 [22] Deng S, Mueller ME, Chan QN, Qamar NH, Dally BB, Alwahabi ZT, et al.
829 Hydrodynamic and chemical effects of hydrogen addition on soot evolution in turbulent
830 nonpremixed bluff body ethylene flames. *Proc Combust Inst* 2017;36:807–14.
831 <https://doi.org/10.1016/j.proci.2016.09.004>.
- 832 [23] Choudhuri AR, Gollahalli SR. Laser induced fluorescence measurements of radical
833 concentrations in hydrogen–hydrocarbon hybrid gas fuel flames. *Int J Hydrogen Energy*
834 2000;25:1119–27. [https://doi.org/10.1016/S0360-3199\(00\)00025-2](https://doi.org/10.1016/S0360-3199(00)00025-2).
- 835 [24] Tesner PA, Robinovitch HJ, Rafalkes IS. The formation of dispersed carbon in
836 hydrocarbon diffusion flames. *Symp (Int) Combust* 1961;8:801–6.
837 [https://doi.org/10.1016/S0082-0784\(06\)80575-8](https://doi.org/10.1016/S0082-0784(06)80575-8).
- 838 [25] Du DX, Axelbaum RL, Law CK. Soot formation in strained diffusion flames with
839 gaseous additives. *Combust Flame* 1995;102:11–20. [https://doi.org/10.1016/0010-2180\(95\)00043-6](https://doi.org/10.1016/0010-2180(95)00043-6).
- 841 [26] Choi J-H, Hwang C-H, Choi SK, Lee SM, Lee WJ, Jang SH, et al. Impacts of hydrogen
842 addition on micro and nanostructure of soot particles formed in C2H4/air counter
843 diffusion flames. *Int J Hydrogen Energy* 2016;41:15852–8.
844 <https://doi.org/10.1016/j.ijhydene.2016.04.158>.

- 845 [27] Gülder ÖL, Snelling DR, Sawchuk RA. Influence of hydrogen addition to fuel on
846 temperature field and soot formation in diffusion flames. *Symp (Int) Combust*
847 1996;26:2351–8. [https://doi.org/10.1016/S0082-0784\(96\)80064-6](https://doi.org/10.1016/S0082-0784(96)80064-6).
- 848 [28] Glassman I. Sooting laminar diffusion flames: Effect of dilution, additives, pressure, and
849 microgravity. *Symp (Int) Combust* 1998;27:1589–96. [https://doi.org/10.1016/S0082-0784\(98\)80568-7](https://doi.org/10.1016/S0082-0784(98)80568-7).
- 851 [29] Guo H, Liu F, Smallwood GJ, Gülder ÖL. Numerical study on the influence of hydrogen
852 addition on soot formation in a laminar ethylene–air diffusion flame. *Combust Flame*
853 2006;145:324–38. <https://doi.org/10.1016/j.combustflame.2005.10.016>.
- 854 [30] Gu M, Chu H, Liu F. Effects of simultaneous hydrogen enrichment and carbon dioxide
855 dilution of fuel on soot formation in an axisymmetric coflow laminar ethylene/air
856 diffusion flame. *Combust Flame* 2016;166:216–28.
857 <https://doi.org/10.1016/j.combustflame.2016.01.023>.
- 858 [31] Sun Z, Dally B, Nathan G, Alwahabi Z. Effects of hydrogen and nitrogen on soot
859 volume fraction, primary particle diameter and temperature in laminar ethylene/air
860 diffusion flames. *Combust Flame* 2017;175:270–82.
861 <https://doi.org/10.1016/j.combustflame.2016.08.031>.
- 862 [32] Zhao H, Stone R, Williams B. Investigation of the soot formation in ethylene laminar
863 diffusion flames when diluted with helium or supplemented by hydrogen. *Energ Fuel*
864 2014;28:2144–51. <https://doi.org/10.1021/ef401970q>.
- 865 [33] Pandey P, Pundir BP, Panigrahi PK. Hydrogen addition to acetylene–air laminar
866 diffusion flames: Studies on soot formation under different flow arrangements. *Combust*
867 *Flame* 2007;148:249–62. <https://doi.org/10.1016/j.combustflame.2006.09.004>.
- 868 [34] De Iuliis S, Maffi S, Migliorini F, Cignoli F, Zizak G. Effect of hydrogen addition on
869 soot formation in an ethylene/air premixed flame. *Appl Phys B* 2012;106:707–15.
870 <https://doi.org/10.1007/s00340-012-4903-2>.
- 871 [35] Haynes BS, Jander H, Mätzing H, Wagner HGg. The influence of gaseous additives on
872 the formation of soot in premixed flames. *Symp (Int) Combust* 1982;19:1379–85.
873 [https://doi.org/10.1016/S0082-0784\(82\)80314-7](https://doi.org/10.1016/S0082-0784(82)80314-7).
- 874 [36] Wei M, Liu J, Guo G, Li S. The effects of hydrogen addition on soot particle size
875 distribution functions in laminar premixed flame. *Int J Hydrogen Energy* 2016;41:6162–
876 9. <https://doi.org/10.1016/j.ijhydene.2015.10.022>.
- 877 [37] Park S-H, Lee K-M, Hwang C-H. Effects of hydrogen addition on soot formation and
878 oxidation in laminar premixed C₂H₂/air flames. *Int J Hydrogen Energy* 2011;36:9304–
879 11. <https://doi.org/10.1016/j.ijhydene.2011.05.031>.
- 880 [38] Liu F, Ai Y, Kong W. Effect of hydrogen and helium addition to fuel on soot formation
881 in an axisymmetric coflow laminar methane/air diffusion flame. *Int J Hydrogen Energy*
882 2014;39:3936–46. <https://doi.org/10.1016/j.ijhydene.2013.12.151>.
- 883 [39] Xu L, Yan F, Wang Y, Chung SH. Chemical effects of hydrogen addition on soot
884 formation in counterflow diffusion flames: Dependence on fuel type and oxidizer
885 composition. *Combust Flame* 2020;213:14–25.
886 <https://doi.org/10.1016/j.combustflame.2019.11.011>.
- 887 [40] Mze Ahmed A, Mancarella S, Desgroux P, Gasnot L, Pauwels J-F, El Bakali A.
888 Experimental and numerical study on rich methane/hydrogen/air laminar premixed
889 flames at atmospheric pressure: Effect of hydrogen addition to fuel on soot gaseous
890 precursors. *Int J Hydrogen Energy* 2016;41:6929–42.
891 <https://doi.org/10.1016/j.ijhydene.2015.11.148>.
- 892 [41] Ezenwajiaku C, Talibi M, Doan NAK, Swaminathan N, Balachandran R. Study of
893 polycyclic aromatic hydrocarbons (PAHs) in hydrogen-enriched methane diffusion

- 894 flames. *Int J Hydrogen Energy* 2019;44:7642–55.
895 <https://doi.org/10.1016/j.ijhydene.2019.01.253>.
- 896 [42] Gaseq Chemical Equilibrium Program n.d. <http://www.gaseq.co.uk/> (accessed February
897 28, 2020).
- 898 [43] Desgroux P, Faccineto A, Mercier X, Mouton T, Aubagnac Karkar D, El Bakali A.
899 Comparative study of the soot formation process in a “nucleation” and a “sooting” low
900 pressure premixed methane flame. *Combust Flame* 2017;184:153–66.
901 <https://doi.org/10.1016/j.combustflame.2017.05.034>.
- 902 [44] Bladh H, Olofsson N-E, Mouton T, Simonsson J, Mercier X, Faccineto A, et al. Probing
903 the smallest soot particles in low-sooting premixed flames using laser-induced
904 incandescence. *Proc Combust Inst* 2015;35:1843–50.
905 <https://doi.org/10.1016/j.proci.2014.06.001>.
- 906 [45] Mouton T, Mercier X, Wartel M, Lamoureux N, Desgroux P. Laser-induced
907 incandescence technique to identify soot nucleation and very small particles in low-
908 pressure methane flames. *Appl Phys B* 2013;112:369–79.
909 <https://doi.org/10.1007/s00340-013-5446-x>.
- 910 [46] Betrancourt C, Liu F, Desgroux P, Mercier X, Faccineto A, Salamanca M, et al.
911 Investigation of the size of the incandescent incipient soot particles in premixed sooting
912 and nucleation flames of n-butane using LII, HIM, and 1 nm-SMPS. *Aerosol Sci
913 Technol* 2017;51:916–35. <https://doi.org/10.1080/02786826.2017.1325440>.
- 914 [47] Aubagnac-Karkar D, El Bakali A, Desgroux P. Soot particles inception and PAH
915 condensation modelling applied in a soot model utilizing a sectional method. *Combust
916 Flame* 2018;189:190–206. <https://doi.org/10.1016/j.combustflame.2017.10.027>.
- 917 [48] Kint JH. A noncatalytic coating for platinum-rhodium thermocouples. *Combust Flame*
918 1970;14:279–81. [https://doi.org/10.1016/S0010-2180\(70\)80040-2](https://doi.org/10.1016/S0010-2180(70)80040-2).
- 919 [49] de Ferrières S, El Bakali A, Gasnot L, Montero M, Pauwels JF. Kinetic effect of
920 hydrogen addition on natural gas premixed flames. *Fuel* 2013;106:88–97.
921 <https://doi.org/10.1016/j.fuel.2012.06.045>.
- 922 [50] Lefort B, El Bakali A, Gasnot L, Pauwels JF. Experimental and numerical investigation
923 of low-pressure laminar premixed synthetic natural gas flames in rich conditions. *Fuel*
924 2017;189:210–37. <https://doi.org/10.1016/j.fuel.2016.10.043>.
- 925 [51] Mercier X, Wartel M, Pauwels J-F, Desgroux P. Implementation of a new spectroscopic
926 method to quantify aromatic species involved in the formation of soot particles in
927 flames. *Appl Phys B* 2008;91:387–95. <https://doi.org/10.1007/s00340-008-2997-3>.
- 928 [52] Mouton T, Mercier X, Desgroux P. Isomer discrimination of PAHs formed in sooting
929 flames by jet-cooled laser-induced fluorescence: application to the measurement of
930 pyrene and fluoranthene. *Appl Phys B* 2016;122:123. <https://doi.org/10.1007/s00340-016-6397-9>.
- 931 [53] Wartel M, Pauwels J-F, Desgroux P, Mercier X. Pyrene measurements in sooting low
932 pressure methane flames by jet-cooled laser-induced fluorescence. *J Phys Chem A*
933 2011;115:14153–62. <https://doi.org/10.1021/jp206970t>.
- 934 [54] Wartel M, Pauwels J-F, Desgroux P, Mercier X. Quantitative measurement of
935 naphthalene in low-pressure flames by jet-cooled laser-induced fluorescence. *Appl Phys
936 B* 2010;100:933–43. <https://doi.org/10.1007/s00340-010-4135-2>.
- 937 [55] Schoemaeker Moreau C, Therssen E, Mercier X, Pauwels JF, Desgroux P. Two-color
938 laser-induced incandescence and cavity ring-down spectroscopy for sensitive and
939 quantitative imaging of soot and PAHs in flames. *Appl Phys B* 2004;78:485–92.
940 <https://doi.org/10.1007/s00340-003-1370-9>.
- 941 [56] Betrancourt C, Mercier X, Liu F, Desgroux P. Quantitative measurement of volume
942 fraction profiles of soot of different maturities in premixed flames by extinction-
943

- 944 calibrated laser-induced incandescence. *Appl Phys B* 2019;125:16.
945 <https://doi.org/10.1007/s00340-018-7127-2>.
- 946 [57] Smith GP, Golden DM, Frenklach M, Moriarty NW, Eiteneer B, Goldenberg M, et al.
947 GRI-Mech 3.0, URL: <http://www.me.berkeley.edu/gri_mech> 51; 1999 p.55 n.d.
- 948 [58] El Bakali A, Mercier X, Wartel M, Acevedo F, Burns I, Gasnot L, et al. Modeling of
949 PAHs in low pressure sooting premixed methane flame. *Energy* 2012;43:73–84.
950 <https://doi.org/10.1016/j.energy.2011.12.026>.
- 951 [59] Yon J, Lemaire R, Therssen E, Desgroux P, Coppalle A, Ren KF. Examination of
952 wavelength dependent soot optical properties of diesel and diesel/rapeseed methyl ester
953 mixture by extinction spectra analysis and LII measurements. *Appl Phys B*
954 2011;104:253–71. <https://doi.org/10.1007/s00340-011-4416-4>.
- 955 [60] Michelsen HA, Liu F, Kock BF, Bladh H, Boiarciuc A, Charwath M, et al. Modeling
956 laser-induced incandescence of soot: a summary and comparison of LII models. *Appl*
957 *Phys B* 2007;87:503–21. <https://doi.org/10.1007/s00340-007-2619-5>.
- 958 [61] Bladh H, Johnsson J, Olofsson N-E, Bohlin A, Bengtsson P-E. Optical soot
959 characterization using two-color laser-induced incandescence (2C-LII) in the soot
960 growth region of a premixed flat flame. *Proc Combust Inst* 2011;33:641–8.
961 <https://doi.org/10.1016/j.proci.2010.06.166>.
- 962 [62] Liu F, Snelling DR, Thomson KA, Smallwood GJ. Sensitivity and relative error analyses
963 of soot temperature and volume fraction determined by two-color LII. *Appl Phys B*
964 2009;96:623–36. <https://doi.org/10.1007/s00340-009-3560-6>.
- 965 [63] Michelsen HA. Understanding and predicting the temporal response of laser-induced
966 incandescence from carbonaceous particles. *J Chem Phys* 2003;118:7012–45.
967 <https://doi.org/10.1063/1.1559483>.
- 968 [64] Appel J, Bockhorn H, Wulkow M. A detailed numerical study of the evolution of soot
969 particle size distributions in laminar premixed flames. *Chemosphere* 2001;42:635–45.
970 [https://doi.org/10.1016/S0045-6535\(00\)00237-X](https://doi.org/10.1016/S0045-6535(00)00237-X).
- 971 [65] Lindstedt RP, Waldheim BBO. Modeling of soot particle size distributions in premixed
972 stagnation flow flames. *Proc Combust Inst* 2013;34:1861–8.
973 <https://doi.org/10.1016/j.proci.2012.05.047>.
- 974 [66] Schuetz CA, Frenklach M. Nucleation of soot: Molecular dynamics simulations of
975 pyrene dimerization. *Proc Combust Inst* 2002;29:2307–14.
976 [https://doi.org/10.1016/S1540-7489\(02\)80281-4](https://doi.org/10.1016/S1540-7489(02)80281-4).
- 977 [67] Eaves NA, Dworkin SB, Thomson MJ. Assessing relative contributions of PAHs to soot
978 mass by reversible heterogeneous nucleation and condensation. *Proc Combust Inst*
979 2017;36:935–45. <https://doi.org/10.1016/j.proci.2016.06.051>.
- 980 [68] Mercier X, Faccinnetto A, Batut S, Vanhove G, Božanić DK, Hróðmarsson HR, et al.
981 Selective identification of cyclopentaring-fused PAHs and side-substituted PAHs in a
982 low pressure premixed sooting flame by photoelectron photoion coincidence
983 spectroscopy. *Phys Chem Chem Phys* 2020;22:15926–44.
984 <https://doi.org/10.1039/D0CP02740E>.
- 985 [69] Faccinnetto A, Irimiea C, Minutolo P, Commodo M, D’Anna A, Nuns N, et al. Evidence
986 on the formation of dimers of polycyclic aromatic hydrocarbons in a laminar diffusion
987 flame. *Commun Chem* 2020;3:1–8. <https://doi.org/10.1038/s42004-020-00357-2>.
- 988 [70] Siegmann K, Sattler K. Formation mechanism for polycyclic aromatic hydrocarbons in
989 methane flames. *J Chem Phys* 1999;112:698–709. <https://doi.org/10.1063/1.480648>.
- 990 [71] Eaves NA, Dworkin SB, Thomson MJ. The importance of reversibility in modeling soot
991 nucleation and condensation processes. *Proc Combust Inst* 2015;35:1787–94.
992 <https://doi.org/10.1016/j.proci.2014.05.036>.

- 993 [72] Kholghy MR, Kelesidis GA, Pratsinis SE. Reactive polycyclic aromatic hydrocarbon
994 dimerization drives soot nucleation. *Phys Chem Chem Phys* 2018;20:10926–38.
995 <https://doi.org/10.1039/C7CP07803J>.
- 996 [73] Mercier X, Carrivain O, Irimiea C, Faccinetto A, Therssen E. Dimers of polycyclic
997 aromatic hydrocarbons: the missing pieces in the soot formation process. *Phys Chem*
998 *Chem Phys* 2019;21:8282–94. <https://doi.org/10.1039/C9CP00394K>.
- 999 [74] Sabbah H, Biennier L, Klippenstein SJ, Sims IR, Rowe BR. Exploring the Role of PAHs
1000 in the Formation of Soot: Pyrene Dimerization. *J Phys Chem Lett* 2010;1:2962–7.
1001 <https://doi.org/10.1021/jz101033t>.
- 1002 [75] Wang H. Formation of nascent soot and other condensed-phase materials in flames. *Proc*
1003 *Combust Inst* 2011;33:41–67. <https://doi.org/10.1016/j.proci.2010.09.009>.
- 1004 [76] Krueger RA, Blanquart G. Predicting aromatic exciplex fluorescence emission energies.
1005 *Phys Chem Chem Phys* 2019;21:10325–35. <https://doi.org/10.1039/C9CP02027F>.
- 1006 [77] Martin JW, Hou D, Menon A, Pascazio L, Akroyd J, You X, et al. Reactivity of
1007 polycyclic aromatic hydrocarbon soot precursors: implications of localized π -radicals on
1008 rim-based pentagonal rings. *J Phys Chem C* 2019;123:26673–82.
1009 <https://doi.org/10.1021/acs.jpcc.9b07558>.
- 1010 [78] Johansson KO, Head-Gordon MP, Schrader PE, Wilson KR, Michelsen HA. Resonance-
1011 stabilized hydrocarbon-radical chain reactions may explain soot inception and growth.
1012 *Science* 2018;361:997–1000. <https://doi.org/10.1126/science.aat3417>.
- 1013 [79] D'Anna A, Violi A, D'Alessio A, Sarofim AF. A reaction pathway for nanoparticle
1014 formation in rich premixed flames. *Combust Flame* 2001;127:1995–2003.
1015 [https://doi.org/10.1016/S0010-2180\(01\)00303-0](https://doi.org/10.1016/S0010-2180(01)00303-0).
- 1016 [80] Frenklach M, Mebel AM. On the mechanism of soot nucleation. *Phys Chem Chem Phys*
1017 2020;22:5314–31. <https://doi.org/10.1039/D0CP00116C>.
- 1018 [81] Adamson BD, Skeen SA, Ahmed M, Hansen N. Detection of Aliphatically Bridged
1019 Multi-Core Polycyclic Aromatic Hydrocarbons in Sooting Flames with Atmospheric-
1020 Sampling High-Resolution Tandem Mass Spectrometry. *J Phys Chem A*
1021 2018;122:9338–49. <https://doi.org/10.1021/acs.jpca.8b08947>.
- 1022 [82] Tang Q, Wang M, You X. Measurements of sooting limits in laminar premixed burner-
1023 stabilized stagnation ethylene, propane, and ethylene/toluene flames. *Fuel*
1024 2019;235:178–84. <https://doi.org/10.1016/j.fuel.2018.07.090>.
- 1025 [83] Singh J, Balthasar M, Kraft M, Wagner W. Stochastic modeling of soot particle size and
1026 age distributions in laminar premixed flames. *Proc Combust Inst* 2005;30:1457–65.
1027 <https://doi.org/10.1016/j.proci.2004.08.120>.

1028
1029

1030

1031 **Figure Captions**

1032 Fig. 1. Impact of hydrogen on flame temperature profiles. Φ -1.82: *CH₄ flame*; Φ -1.82_H2-S:
1033 *CH₄ substituted-H₂ flame*; Φ -1.82_H2-A: *CH₄ added-H₂ flame* (see Table 1 for the flame
1034 conditions).

1035 Fig. 2. Mole fraction profiles of reactants (fuel, O₂) and major products (CO, CO₂, H₂, H₂O)
1036 as a function of the distance from the burner surface, obtained in the three studied flames..

1037 Fig. 3. Graphical summary of the normalized maximum mole fractions of the soot precursors
1038 measured in the three studied flames. Normalization has been performed, species by species,
1039 regarding to the highest mole fraction value measured in the three flames.

1040 Fig. 4. Mole fraction profiles of selected aliphatic species considered as soot precursors:
1041 acetylene, propyne and 1-butyne obtained in the three studied flames.

1042 Fig. 5. Mole fraction profiles of benzene, naphthalene and pyrene obtained in the three studied
1043 flames.

1044 Fig. 6. Possible chemical paths characterizing the kinetic impact of hydrogen atoms in sooting
1045 flames. Species written with a star are radicals.

1046 Fig. 7. LII temporal signals measured at different distances from the burner surface in the
1047 three studied flames: **(a)** CH₄ flame (Φ -1.82), **(b)** CH₄ substituted-H₂ flame (Φ -1.82_H2-S),
1048 **(c)** CH₄ added-H₂ flame (Φ -1.82_H2-A). For clarity, the peak of LII signals have been
1049 normalized to 1. Laser fluence was set at 0.415 J cm⁻². **(d)** LII decay-times measured at 1/e of
1050 the LII signal as a function of the distance from the burner surface.

1051 Fig. 8. Profiles of benzene, naphthalene and pyrene mole fraction, soot volume fraction and
1052 temperature obtained in the studied flames. The line at 9 mm is drawn to guide the eye
1053 regarding the starting point of soot formation.

1054 Fig. 9. Influence of H₂ on the relationship between the soot volume fraction and the squared
1055 concentration of benzene, naphthalene, and pyrene ($[C_6H_6]^2$, $[C_{10}H_8]^2$ and $[C_{16}H_{10}]^2$)
1056 respectively **(a)** and the product of the concentrations of two different PAHs
1057 ($[C_6H_6] \times [C_{10}H_8]$, $[C_6H_6] \times [C_{16}H_{10}]$, $[C_{10}H_8] \times [C_{16}H_{10}]$) **(b)** in the soot inception zone of
1058 flames Φ -1.82 and Φ -1.82_H2-A. Flame Φ -1.82: left *and* bottom axes. Flame Φ -1.82_H2-A:
1059 right and *top axes*.

1060